NASA TECHNICAL REPORT

NASA TR R-424

NASA TR R-424

OPTICAL HOLOGRAPHY APPLICATIONS FOR THE ZERO-g ATMOSPHERIC CLOUD PHYSICS LABORATORY

by Robert L. Kurtz

George C. Marshall Space Flight Center
Marshall Space Flight Center, Ala. 35812

NATIONAL AERONAUTICS AND SPACE ADMINISTRATION • WASHINGTON, D. C. • MAY 1974

1. REPORT NO.	2. GOVERNMENT ACCESSION NO.	3. RECIPIENT'S CATALOG NO.
NASA TR R-424		

4. TITLE AND SUBTITLE	5. REPORT DATE
Optical Holography Applications for the Zero-g Atmospheric Cloud Physics Laboratory	May 1974
	6. PERFORMING ORGANIZATION CODE
7. AUTHOR(S)	8. PERFORMING ORGANIZATION REPORT #
Robert L. Kurtz	M463
9. PERFORMING ORGANIZATION NAME AND ADDRESS	10. WORK UNIT NO.
George C. Marshall Space Flight Center Marshall Space Flight Center, Alabama 35812	645-10-01-0000
	11. CONTRACT OR GRANT NO.
	13. TYPE OF REPORT & PERIOD COVERED
12. SPONSORING AGENCY NAME AND ADDRESS	Technical Report
National Aeronautics and Space Administration Washington, D.C. 20546	14. SPONSORING AGENCY CODE

15. SUPPLEMENTARY NOTES

Prepared by Space Sciences Laboratory, Science and Engineering

16. ABSTRACT

A complete description of holography is provided, both for the time-dependent case of moving scene holography and for the time-independent case of stationary holography. Further, a specific holographic arrangement is proposed for application to the detection of particle size distribution in an atmospheric simulation cloud chamber. In this chamber particle growth rate is investigated; therefore, the proposed holographic system must capture continuous particle motion in real time. Such a system is described.

17. KEY WORDS	18. DISTRIBUTION STATEMENT
Cloud physics Holographic particle sizing Motion holography	CAT. 13

19. SECURITY CLASSIF. (of this report)	20. SECURITY CLASSIF. (of this page)	21. NO. OF PAGES	22. PRICE
Unclassified	Unclassified	76	$4.00

MSFC - Form 3238 (Rev December 1972)

For sale by National Technical Information Service, Springfield, Virginia 22151

FOREWORD

Holography appears to have the potential of providing a unique measurement procedure for use in cloud microphysical research because of its ability to capture and reproduce a three-dimensional image of an event without interfering with the event. The motion, velocity, and growth cycles of particles can be recorded in a manner not obtainable with standard photographic techniques used in most cloud physics research programs. The study reported herein resulted from meetings and discussions with the author and Mr. William W. Vaughan, Chief, Aerospace Environment Division, Aero-Astrodynamics Laboratory, Marshall Space Flight Center, and others engaged in feasibility studies for a zero-gravity (zero-g) atmospheric cloud physics laboratory as a payload for the Space Shuttle/Spacelab. The study documented by this report was made to investigate the feasibility of applying holographic techniques to the real-time determination of atmospheric cloud particles parameters in a zero-g environment.

The Zero-g Atmospheric Cloud Physics Laboratory is being developed under the technical direction of the Marshall Space Flight Center on behalf of the NASA Office of Applications and the Office of Manned Space Flight. The primary objective of this program is to provide a multi-experiment laboratory which members of the cloud physics scientific community may use in their research of cloud microphysical processes. Emphasized will be processes for which a near zero-g environment will enhance their capability to improve our current knowledge for application to cloud physics and weather modification problems.

William W. Vaughan
Project Manager
Zero-g Atmospheric Cloud
Physics Laboratory Project

TABLE OF CONTENTS

LIST OF ILLUSTRATIONS

LIST OF ILLUSTRATIONS (Concluded)

OPTICAL HOLOGRAPHY APPLICATIONS FOR THE ZERO-g ATMOSPHERIC CLOUD PHYSICS LABORATORY

INTRODUCTION

Statement of the General Problem

The science of meteorology has advanced rapidly toward the development of an understanding of large-scale atmospheric processes. Large-scale flow patterns in the atmosphere can be predicted with reasonable success because of the progress in defining and refining the equations of motion and conservation of mass and momentum. These large-scale flow patterns enable one to define and predict patterns of cloudiness. This cloudiness itself, the processes in the clouds, and the redistribution and release of energy in the clouds are what the average citizen thinks of as weather.

In nature there are many cubic kilometers of clouds. Most cloud elements are inside the cloud and are not affected by the edges of the cloud. A terrestrial experimenter has the problem of trying to duplicate a system in which there are no edge effects and in which a cloud can survive long enough to have a number of things happen to it. The smallest of these cloud particles fall at several centimeters per second, and as they grow they reach fall velocities above 1 m/sec. This means that in a terrestrial cloud chamber that is 1 m in the vertical dimension, there is less than 1 sec of observational time for the larger of these particles. Attempts to overcome this limitation include capturing individual particles and placing them on wax paper, Teflon, copper, or stainless steel surfaces; hanging them on a thermocouple; suspending them on a spider web or a thread; or placing them between two immiscible liquids. These approaches have not been very successful because the suspension medium generally causes effects greater than the forces or actions that are being measured.

Many significant accomplishments have been made in terrestrial laboratories. However, a comparison between the results achieved in the laboratory and what is observed in nature often gives no correlation whatsoever. In studying the whole regime of meteorology from the large-scale motions which produce cloud systems down to what is called weather (i.e., rain, snow, lightning), there are gaps in understanding the microphysical processes that occur between the inception of the cloud system formation and the events eventually occurring at the ground. Many of these data lie in the area called cloud physics. Meteorologists have long understood the requirement for a much better understanding of cloud microphysics. For the last 30 yr concentrated efforts have been made to understand some of the following atmospheric processes: Why does one cloud develop a spectrum of broad droplet sizes while others develop narrow spectra of sizes? Why does one cloud precipitate and others do not? Why does one cloud develop rapid electrical charging, charge separation, lightning and thunder, while other clouds

similar in outward appearance do not? Why does one thunderstorm produce hail and another not? Why does a field of thousands of clouds produce hundreds of moderate thunderstorms, but only one develops into a tornado? Microphysicists, physical chemists, and applied physicists, as well as meteorologists, are still heavily involved in the study of the phenomena associated with these atmospheric processes.

The range of cloud physics laboratory research extends from the millimeter rain drops and ice crystals to submicrometer condensation nuclei. Nature requires at least a million 10-μm-diameter cloud drops to combine in order to produce a 1-mm-diameter precipitation drop. These droplets possess certain surface, electrical, and aerodynamic properties which establish whether these million small drops can combine to form the one big drop. Individual ice crystals must also be studied to determine how they grow and whether these ice crystals will somehow splinter and multiply to form more ice crystals. Other problems include electrical charging of ice crystals during the growth and collision processes and the effect of this charging on thunderstorm electrification. Many microphysical processes have been studied in some detail in the laboratory but under conditions which are not very representative of those in a cloud. In any cloud, the average element or group of elements within that cloud has a lifetime of approximately 20-min during which these cloud particles will grow and perhaps evaporate again.

Cloud physics research under zero-gravity (zero-g) or low-g conditions offers solutions to many of these problems. Under zero-g conditions, the experimenter can place a drop in a chamber and observe it through a microscope for long periods of time. The droplet can be frozen, thawed, and another drop propelled into it. The migration and collection of particulates that may be near or around the drop can be observed. Numerous experiments (e.g., determining whether a freezing drop splinters and/or acquires a charge) can be done in this unique environment that cannot be done on earth. Other important experimental areas include the diffusional growth of drops and ice crystals and studies of the effect of temperature on an ice crystal's type and form.

In the study of cloud physics one is primarily interested in and working with particles of some form and size. The physical parameters of the particles of interest are many and varied. With regard to physical size, the particles of concern to the cloud physicist fall into basically two categories: (1) the condensation nuclei, which range from 0.1 μm to about 1 μm, and (2) the giant nuclei, which include all particles greater than 1 μm. The total particle size spectrum of interest is presented in Figure 1. Figure 2 presents some of the experimental chambers currently under consideration for the Zero-g Atmospheric Cloud Physics Laboratory proposed for the Shuttle/Spacelab Program.

This zero-g-type atmospheric laboratory has been conceived to provide the cloud physics scientific community with a general-purpose laboratory for furthering their basic understanding of cloud microphysical processes. During the course of the Zero-g Atmospheric Cloud Physics Laboratory feasibility study [1, 2, 3], it was recognized that techniques to photograph and observe the events occurring during the experiments must be identified and that studies should be performed to select the best technique or

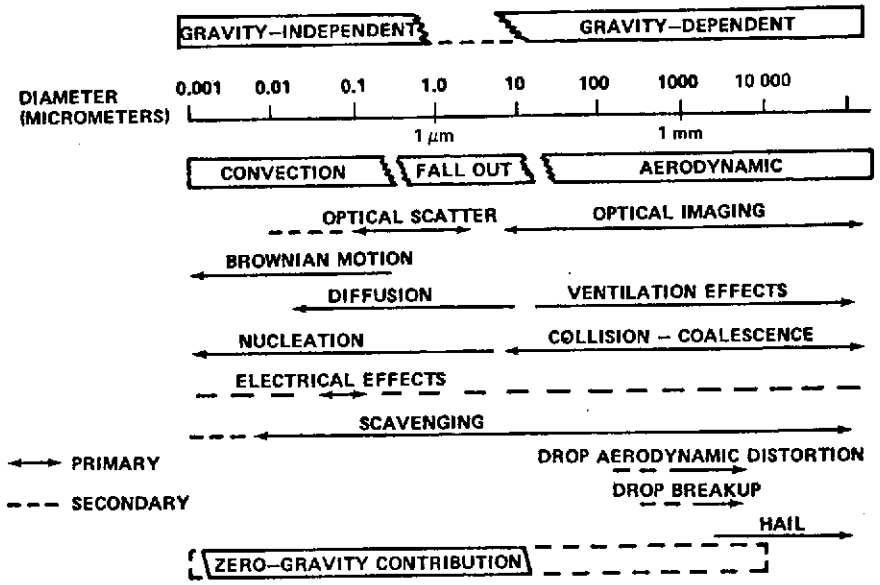

Figure 1. Particle size spectrum.

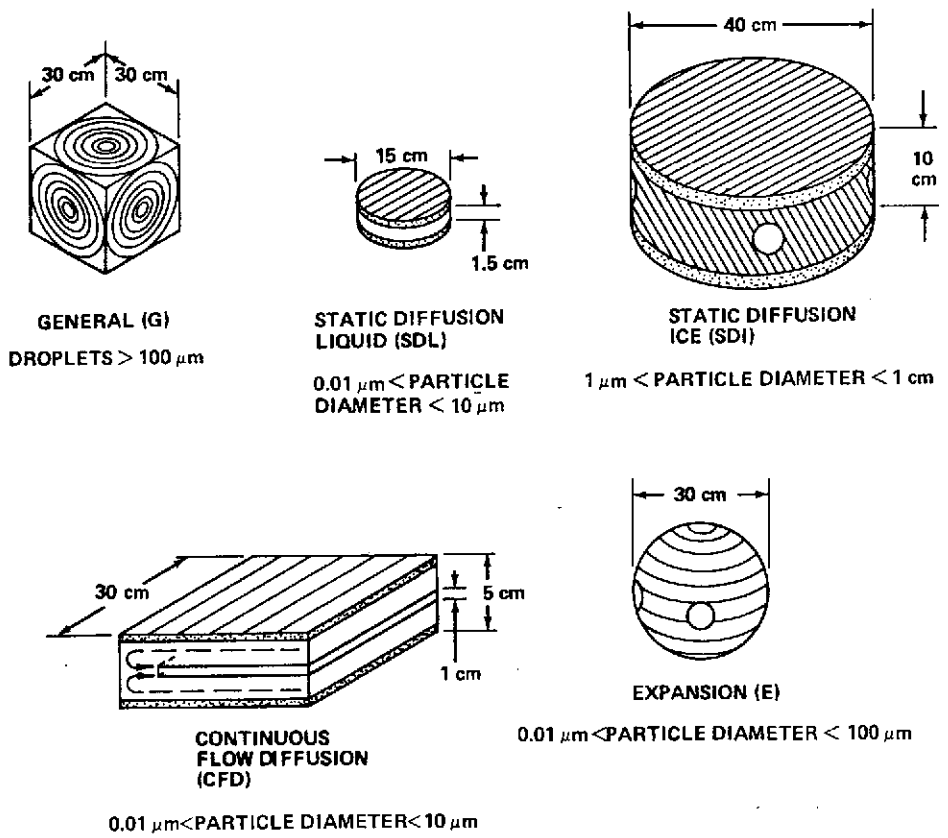

Figure 2. Proposed atmospheric cloud physics chambers.

combination of techniques to accomplish the data management. Since holography has the unique capability to record large amounts of data that cannot be obtained by other techniques, a study was undertaken to determine which holographic system would be best for use with the Zero-g Atmospheric Cloud Physics Laboratory program. This report presents the results of the studies accomplished thus far.

Specific Objectives of the Study

The objective of this study was to investigate the feasibility of applying holographic techniques to the real-time determination of particle parameters in a zero-g environment. Such feasibility would be judged, of course, in a 1-g laboratory environment, with the primary constraints of particle resolution and velocity being imposed on the proposed holographic technique. The particle parameters to be determined holographically were

1. Particle Size
2. Particle Size Distribution
3. Particle Velocity of Motion
4. Particle Velocity Distribution
5. Particle Growth
6. Particle Growth Rate
7. Particle Trajectories
8. Particle Deformation.

If the environment or particle field of interest is static or dynamic and involves a reasonable volume, holography provides a tailor-made technique for the real-time detection, observation, and measurement of various physical parameters of the individual particles within the volume. Consequently, holography can provide much of the necessary information about the total content of the particle field. That holography is a tailor-made technique for such particle field investigations is evidenced by the fact that it allows the entire particle field volume of interest to be recorded on one exposure. Upon reconstruction of the hologram, one may inspect the recorded volume of interest for the investigation of the physical parameters of concern at any later, more convenient time. For example, consider that the astronaut experimenter has recorded a hologram during an experiment while in orbit. Upon reconstruction of this hologram in an earth laboratory, all observers would see exactly and precisely what the astronaut saw and recorded during the experiment.

Today there are numerous applications of holography to the problem of real-time particle detection. Some examples are fog and rain evaluation, wind-tunnel studies, rocket-exhaust analysis, pollution monitoring, and Skylab waste-tank analysis. Most of these previous applications employed the technique of in-line holography, which will be discussed in the following section.

DESCRIPTION OF THE GENERAL HOLOGRAPHIC TECHNIQUE

Introduction

In general, if information on particles and particle parameters is desired from any given environment or particle field, one must resort to experimental techniques to determine particle parameter information. These environments or particle fields of interest may be anything from ordinary smokestacks, which produce common air pollutants, to the analysis of rocket exhaust, to wind-tunnel studies, to fog and rain evaluation, or to the present environment of particle fields within a controlled cloud physics chamber.

As mentioned earlier, one of the first holographic techniques applied to such particle field investigations was the technique of in-line holography. With the aid of Figure 3, this technique may be described in the following way. A plane wave-front beam is incident on and passes through some target volume of interest. The presence of individual particles distributed throughout this volume essentially causes the plane wave to become scattered and diffracted at many points so as to produce a spherical wave as well as a plane wave. The plane wave is, of course, that part of the incident wave which passes through the target field region undisturbed. This undisturbed plane wave then constitutes the holographic reference beam. The spherical wave produced by the scattering and diffraction around the individual particles constitutes the holographic object beam. These two waves interfere at the film plane, and the interference pattern so recorded at the film plane provides the means for reconstructing the real image of the target field region. An inspection of this real image provides quantitative information about the individual particles that make up the target field. The basic problem with the in-line system is that for high-density particle fields, the reference beam is excessively attenuated, and the observer or detector must look directly back into the laser source on reconstruction.

The optical holographic system to be considered for application to the Zero-g Atmospheric Cloud Physics Laboratory program will be a modified acute sideband technique. Some basic descriptions of sideband holographic techniques, both for the stationary and moving object fields, will now be presented. These basic concepts are provided so that this study of an optical holographic technique can stand alone.

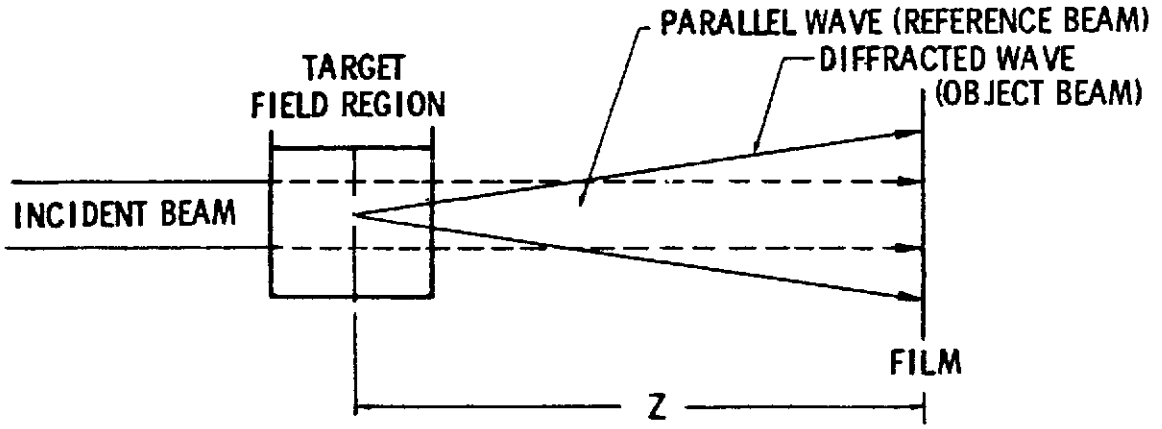

Figure 3. In-line holography.

General Description of Sideband Holography for a Stationary Scene

Let the plane of the hologram lie in the x-y plane of the coordinate system, as given in Figure 4. The amplitude in this plane can be described by the radiation from the scene,

$$E_s = b\,(x,y)\exp\left\{i[\beta(x,y) - \omega t]\right\} \quad , \tag{1}$$

and by that of the reference beam,

$$E_r = a(x,y)\exp\left\{i[\alpha(x,y) - \omega t]\right\} \quad . \tag{2}$$

The amplitude functions, b (x,y) and a (x,y), and the phase functions, $\alpha(x,y)$ and $\beta(x,y)$, are considered to be real functions. This, then, is a scalar treatment that does not take account of polarization effects. However, it is always possible to split the scene wave into two components, one with the electric vector in the plane containing the electric vector and the direction of propagation of the reference ray and the other with the electric vector perpendicular to this plane. Only the parallel component contributes to the interference pattern on the hologram and, hence, to the reconstruction. Furthermore, a(x,y) is a slowly variable function (a constant for a plane reference wave but, for a spherical wave, it varies as the reciprocal of distance from the reference source to different points on the hologram). The reference wave may also be a distorted spherical

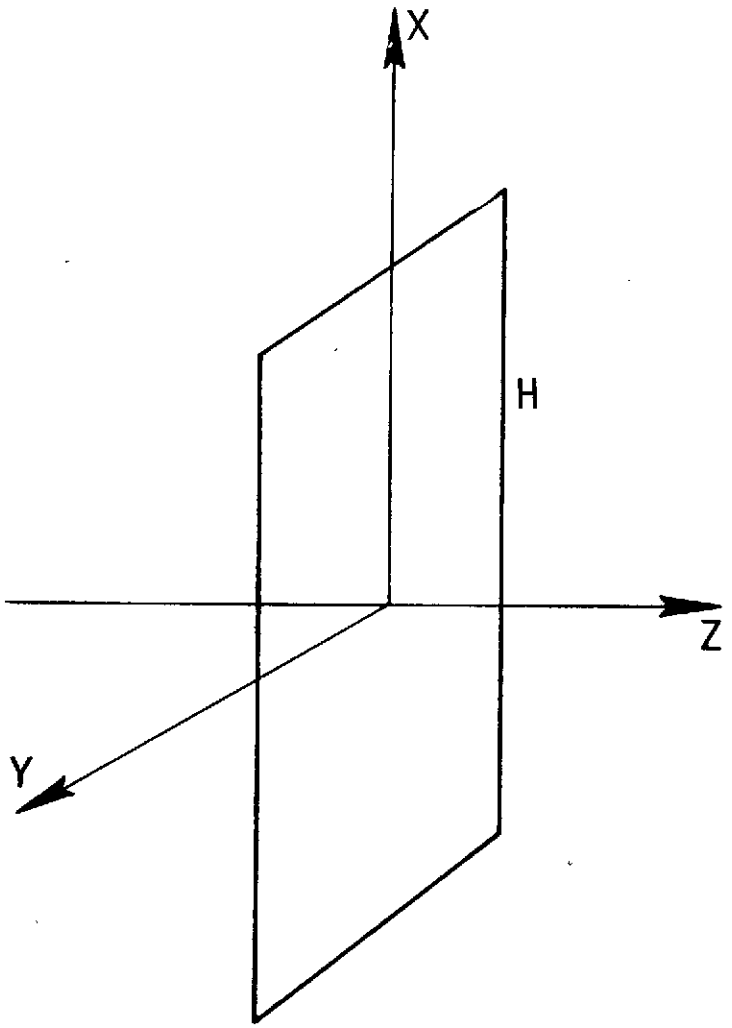

Figure 4. Coordinate system.

wave, as formed by a lens with geometrical aberrations. The amplitude function of the scene (object) wave, b(x,y), is materially smaller than a(x,y) since the ratio of intensity of the reference beam to that of the scene beam is usually required to be from 3 to 1 to 10 to 1. The exposure on the hologram plate is given by the product of the intensity at the plate times the time of exposure, or pulse length.

In general, from the definition of Poynting's vector in the rationalized meter-kilogram-second system

$$\vec{S} \equiv \vec{E} \times \vec{H}$$

one can see that its time average is

$$\langle \vec{S} \rangle = \langle \vec{E} \times \vec{H} \rangle = 1/2 \sqrt{\epsilon/\mu}\, EE^* \hat{n} \quad , \tag{3}$$

where E^* is the complex conjugate of E, and $\hat{n}$ is a unit vector, mutually perpendicular to $\vec{E}$ and $\vec{H}$. Since the intensity (i.e., irradiance) of electromagnetic radiation is the energy crossing normal to a unit area per unit time,

$$I = \langle S \rangle = 1/2 \sqrt{\epsilon/\mu}\, EE^* = 1/2\, Z\, EE^* = m\, EE^* \quad , \tag{4}$$

where $Z = \sqrt{\mu/\epsilon}$ is the impedance of the medium, and m is a constant for simplification. For a hologram,

$$I = m\, EE^* = m\, (E_r + E_s)\, (E^*_r + E^*_s) \quad , \tag{5}$$

and from equations (1) and (2),

$$I = m \left\{ b\,(x,y)\, e^{i[\beta\,(x,y) - \omega t]} + a\,(x,y)\, e^{i[\alpha\,(x,y) - \omega t]} \right\} \cdot \left\{ b\,(x,y)\, e^{-i[\beta\,(x,y) - \omega t]} + a\,(x,y)\, e^{-i[\alpha\,(x,y) - \omega t]} \right\} \tag{6}$$

or

$$I = m \left\{ b^2(x,y) + a^2(x,y) + a(x,y)\, b(x,y) \left[e^{i[\beta\,(x,y) - \alpha\,(x,y)]} + e^{-i[\beta\,(x,y) - \alpha\,(x,y)]} \right] \right\} \quad , \tag{7}$$

where equation (7), for the intensity recorded at the plate, is generally called the recording equation.

Now the substitution of equation (7) into the equation for the exposure produces

$$\mathcal{E} = \int_0^\tau \bar{I}\, dt = m \int_0^\tau b^2(x,y) + a^2(x,y) + 2a(x,y)\, b(x,y) \cos(\beta - \alpha)\, dt$$

or

$$It = m\tau [b^2(x,y) + a^2(x,y) + 2a(x,y)\, b(x,y) \cos(\beta - \alpha)] \tag{8}$$

but τ is just some constant exposure time, τ_0, for a given hologram; therefore, the exposure may be simply written as

$$It = m\tau_0 [a^2 + b^2 + 2ab \cos(\beta - \alpha)]$$

where a, b, α and β are coordinate dependent, or

$$It = m\tau_0 \left\{ a^2 + b^2 + ab \left[e^{i(\beta - \alpha)} + e^{-i(\beta - \alpha)} \right] \right\} \tag{9}$$

It is well known in photography that the Heurter-Driffield characteristic curve as plotted on the semilog plate is linear for most of its length and can be represented in this linear region by

$$D = \gamma \log \frac{It}{g}$$

where D is the density of the image on the film, γ is the contrast, and g is the inertia of the emulsion. Since

$$D \equiv -\log T \quad ,$$

$$T = g^{\gamma} (I\tau)^{-\gamma} \tag{10}$$

where T is the transmission coefficient. The amplitude transmission coefficient, T_a, is the square root of the transmission; consequently,

$$T_a = g^{\gamma/2} (I\tau_0)^{-\gamma/2} = kI^{-\gamma/2} \quad , \tag{11}$$

where $k \equiv (g/\tau_0)^{\gamma/2}$ is a constant and

$$T_a = k\left\{a^2 + b^2 + ab\left[e^{i(\beta - \alpha)} + e^{-i(\beta - \alpha)}\right]\right\}^{-\gamma/2} \quad . \tag{12}$$

Factoring,

$$T_a = (k)\,(a^2 + b^2)^{-\gamma/2}\left[1 + \frac{ab}{a^2 + b^2}\, e^{i(\beta - \alpha)} + e^{-i(\beta - \alpha)}\right]^{-\gamma/2} \quad . \tag{13}$$

Binomial expansion may be used to obtain

$$T_a = k(a^2 + b^2)^{-\gamma/2}\left\{1 - \frac{\gamma}{2}\,\frac{ab}{a^2 + b^2}\left[e^{i(\beta - \alpha)} + e^{-i(\beta - \alpha)}\right] + \text{higher-order terms}\right\} \quad . \tag{14}$$

However, by careful development of the exposed plate, one obtains a positive transparency with an overall gamma of ($\gamma = -2$), which yields

$$T_a = k(a^2 + b^2)\left\{1 + \frac{ab}{a^2 + b^2}\left[e^{i(\beta - \alpha)} + e^{-i(\beta - \alpha)}\right]\right\} \quad , \tag{15}$$

and higher-order terms are omitted because they are negligibly small compared with one.

Consider the usual case where the reference beam during reconstruction is essentially identical with that during recording. Let this reference wave be incident on the developed hologram; just beyond the hologram the wave amplitude is

$$E_t = T_a E_r \quad . \tag{16}$$

Then, from equations (2) and (15),

$$E_t = \left[ka\,(a^2 + b^2)\right] \left\{ e^{i(\alpha - \omega t)} + \frac{ab}{a^2 + b^2} \left[e^{i(\beta - \omega t)} + e^{-i(\beta - 2\alpha + \omega t)} \right] \right\}. \tag{17}$$

The first term,

$$ka\,(a^2 + b^2)\, e^{i(\alpha - \omega t)} \quad , \tag{18}$$

is then simply the reference beam attenuated by a term proportional to $(a^2 + b^2)$; therefore, the first term is

$$k\,(a^2 + b^2)\, E_r \quad . \tag{19a}$$

The second term,

$$\left[ka\,(a^2 + b^2)\right] \left[\frac{ab}{(a^2 + b^2)}\, e^{i(\beta - \omega t)} \right] \quad ,$$

becomes

$$ka^2\,(b\, e^{i(\beta - \omega t)} = k\, a^2\, E_s \quad , \tag{19b}$$

which corresponds to the original wave, equation (1) multiplied by the same shading factor as for the reference beam. One may infer from the form of the second term that upon viewing through the hologram, illuminated by the reference beam, one should see this virtual image of the object in the precise position previously occupied by the object with reference to the original position of the hologram. If the hologram is in its same position after reconstruction, the image of the object will be precisely superimposed on the actual object. However, the brightness of the image will be slightly reduced.

The third term,

$$k\,a^2\,b\,e^{-i(\beta - 2\alpha + \omega t)} = k\,a^2\,b\,e^{i2(\alpha - \beta) + i(\beta - \omega t)}$$

becomes

$$k\,a^2\,e^{i2(\alpha - \beta)}\,E_s \quad , \tag{19c}$$

which corresponds to the real image of the object and is located on the opposite side of the hologram plate from the virtual image. This real image is not aberration free and is, therefore, termed pseudoscopic.

Theoretical Description of Time-Dependent Holography

The previous section was useful to show, mathematically, how a hologram is able to reconstruct a three-dimensional image of a real object by the reconstruction of the various wave fronts. We now intend to show that if the real object moves during the exposure of the hologram, the wave fronts become time dependent. For example, in the present problem of the zero-g cloud physics chambers, the particle field of the environment will be in constant motion. The effect of this object motion on the reconstructed wave front, i.e., the holographic image, must be determined. This information will allow determination of whether it is feasible to expect to record holographically such moving particle fields.

From the previous section, the basic exposure equation may be written as:

$$\mathcal{E}(P) = m \int_{-\tau/2}^{\tau/2} \left\{ E_r^2 + E_s^2 + 2\,E_r\,E_s \cos k\,[s(P) - r(P)] \right\} dt \quad . \tag{20}$$

It must now be determined whether the holographic system is to become time dependent or time independent. A time-dependent system will be considered first. This time dependence is permitted by having the object (e.g., a particle) moving during the exposure. Then during the hologram exposure, s(P), which is the object beam path length in equation (20), becomes

$$s(P) = s_p(t) \quad , \tag{21}$$

and equation (20) for the exposure becomes

$$\mathcal{E}(P) = m\tau\left\{E_r^2 + E_s^2 + \frac{2E_r E_s}{\tau}\int_{-\tau/2}^{\tau/2} \cos k\left[s_p(t) - r(P)\right] dt\right\} \quad . \tag{22}$$

Therefore, the time dependence arrives as a result of the time-dependent path length change of the object beam caused by the motion of the object or particle. To proceed further, one must be able to completely specify the path length change s(t). For this discussion, consider the object or particle to have linear motion over some distance s during the time of exposure. Then, in general,

$$\frac{ds}{dt} = v \quad , \tag{23}$$

and integrating,

$$s(t) = s_o + vt \quad . \tag{24}$$

The diagram for this very special case of the time dependence of s(t), along the line of the original s, is given in the Appendix, where the more rigorous vector description of this time dependency of motion is presented. The purpose here is only to demonstrate the dependence of motion holography on the system geometry. Substituting equation (24) into equation (22) produces

$$\mathcal{E}(P) = m\tau\left[K_C + \frac{2E_r E_s}{\tau}\int_{-\tau/2}^{\tau/2} \cos(kvt + \phi)\right] \tag{25}$$

where $K_C = E_r^2 + E_s^2$ and $\phi = k\,(s_0 - r) \neq f(t)$. Performing the indicated integration of equation (25),

$$\mathcal{E}(P) = m\tau\left(K_C + 2E_r E_s \operatorname{sinc} kv\,\tau/2 \cos\phi\right) \tag{26}$$

where $\operatorname{sinc} kv\,\tau/2 = [\sin kv(\tau/2)]/[kv(\tau/2)]$.

Equation (26) becomes the exposure equation for the time-dependent case of linear motion of a particle. Recall that equation (20) is the exposure equation for the time-independent case of the stationary particle. For this time-independent case, simply let

$$[s(P) - r(P)] = \phi$$

and integrate over dt to obtain

$$\mathcal{E}(P) = m\tau\left(K_C + 2E_r E_s \cos\phi\right) \tag{27}$$

as the final exposure relation for the time-independent case.

If the particle velocity were zero, then the exposure expression of equation (26) should simply reduce to that of equation (27) for the stationary case. Setting $v = 0$ in equation (26), one need only treat

$$\operatorname{sinc} kv\,\tau/2 = \lim_{v \to 0} \operatorname{sinc} kv\,\tau/2 \equiv 1 \quad , \tag{28}$$

and, indeed, equation (26) does reduce to equation (27) as expected.

Therefore, the time dependence of holography is determined by the path length change of the object beam during the exposure. This change of path length is then reflected as an amplitude modulation of the phase term, $\cos\phi$, in the exposure relation.

It must be pointed out here that this change in path length of the object beam is a function of the direction of the motion vector for the object or particle with respect to the vector for the path length of the object beam. Because the path length change of the object beam results in a relative phase change between object and reference beam, the following section is presented.

Dependence of Relative Phase Shift on the Geometry of the Holographic Arrangement

It has been shown that the time dependence of motion holography results from the path length change which occurs in the object beam because of the total motion of the object or particle during the exposure. Because holography is an interference phenomenon, the total change in path length, Δd, of the object beam during the exposure must be less than $\lambda/2$ (i.e., $k\lambda/2 = \pi$). Because of this severe restriction, the geometry of the optical arrangement used becomes of utmost importance to the successful recording of a moving object or particle. Attention, therefore, is directed to two limiting cases of sideband geometry.

Consider the holographic arrangement of Figure 5. This constitutes a very desirable arrangement for a stationary object because of the high energy return from the object to the film plate. For this case, the radiation propagation vector $\bar{k}$ is both parallel and antiparallel to the direction of the intended object motion, Δx. Consider that during the exposure the object moves from position x_0 to a new position x_1; we call this object translation Δx. Then the total optical path length change is

$$\Delta d = 2\,\Delta x \quad ; \tag{29}$$

yet, using the limiting requirement for the allowed change in optical path length of a holographic arrangement,

$$\Delta d < \lambda/2 \tag{30}$$

or

$$\Delta x < \lambda/4 \quad , \tag{31}$$

and the object cannot travel a total distance greater than $\lambda/4$ if a hologram is to be successfully recorded. This was an obvious result when the object motion, Δx, was allowed to be along the direction of the radiation propagation vector, $\bar{k}$. This geometry allows the minimum amount of object motion during the exposure.

A contrasting case is given in Figure 6. The basic difference in geometry between this and the previous arrangement is the rotation of one mirror. Everything is as before except that now the direction of motion, Δx, of the object is perpendicular to the

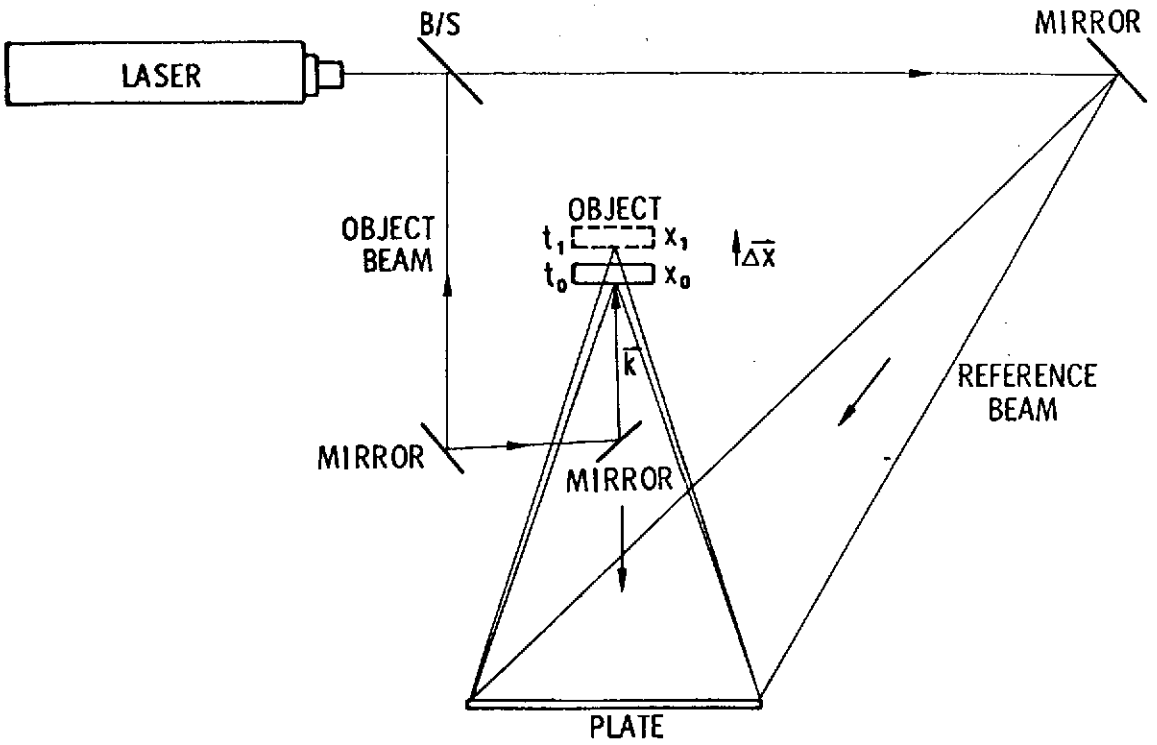

Figure 5. Maximum sensitivity sideband holographic arrangement.

propagation vector, $\vec{k}$. The result is, of course, that now the magnitude of Δx may be as large as desired without any change occurring in the object beam path length. For this geometrical arrangement,

$$\Delta d \equiv 0 \quad . \tag{32}$$

Of course, if one expects to resolve the object in the hologram with such an arrangement, the allowed Δx is not totally unlimited. As a rule of thumb, it may not travel further than one-tenth of its length during the exposure because of resolution requirements. But this is an unusually large distance compared with $\lambda/2$. The price paid for this large motion is that no resolution of front-surface detail has been recorded. The image simply appears as a black silhouette against a lighted background.

A unique geometrical arrangement has been conceived which provides the advantages of both of the previous limiting cases and apparently does so without the concomitant disadvantages of these systems [4–10]. This new system allows the

resolution of front-surface detail to be recorded from a moving object, gives maximum utilization of the available coherence length, and allows sufficiently large object motion, Δx, during the exposure to capture moving objects with velocities of extreme magnitude.

Consider the ellipse of Figure 7. The three paths shown are all of constant length and equal to twice the value of the semimajor axis. This fact of constancy proves to be quite beneficial for the geometry.

Suppose one could cause the object or particle of interest to move along the surface of such an ellipse. The laser source could then be positioned at one focus and the film recorder at the other. In this way, regardless of the total motion during the hologram exposure, the object beam path length would always be constant and equal to 2a. Further, one could always front illuminate the object or particle. From a practical point of view, such an elliptical motion trajectory is not very useful. The situation previously described can be approximated, however, by allowing the motion vector for the object to be tangent to the surface of the ellipse. If the motion is considered to be linear, then the linear motion vector must be parallel to the semimajor axis of the ellipse and perpendicular to the semiminor axis. In this way a straight line is used to approximate the surface of the ellipse. It turns out that the approximation is quite good over a small section of the ellipse surface [3]. This statement is verified by the ability to reconstruct a hologram of an object in constant motion during exposure [4]. This system has been used to successfully record a hologram of an object having total motion, Δx, equal to 10 000 wavelengths of the source radiation while allowing less than one-half wavelength changes in the object beam path length [9].

Some Technical Aspects of Image-Recorder Resolution and Effects of Recorder Size

The point of view taken for the discussions here will follow that of Collier, et al. [11]. Consider the constant subject-reference phase difference of holography caused by the finite extension of the subject. The bright fringes of the interference pattern occur when

$$\Delta \ell = n\lambda_1 \quad , \tag{33}$$

where n is an integer and $\Delta \ell$ is the constant path difference of point references between subject and reference beams.

From the basic consideration of the concentric in-line system of Reference 11, equation 3.5,

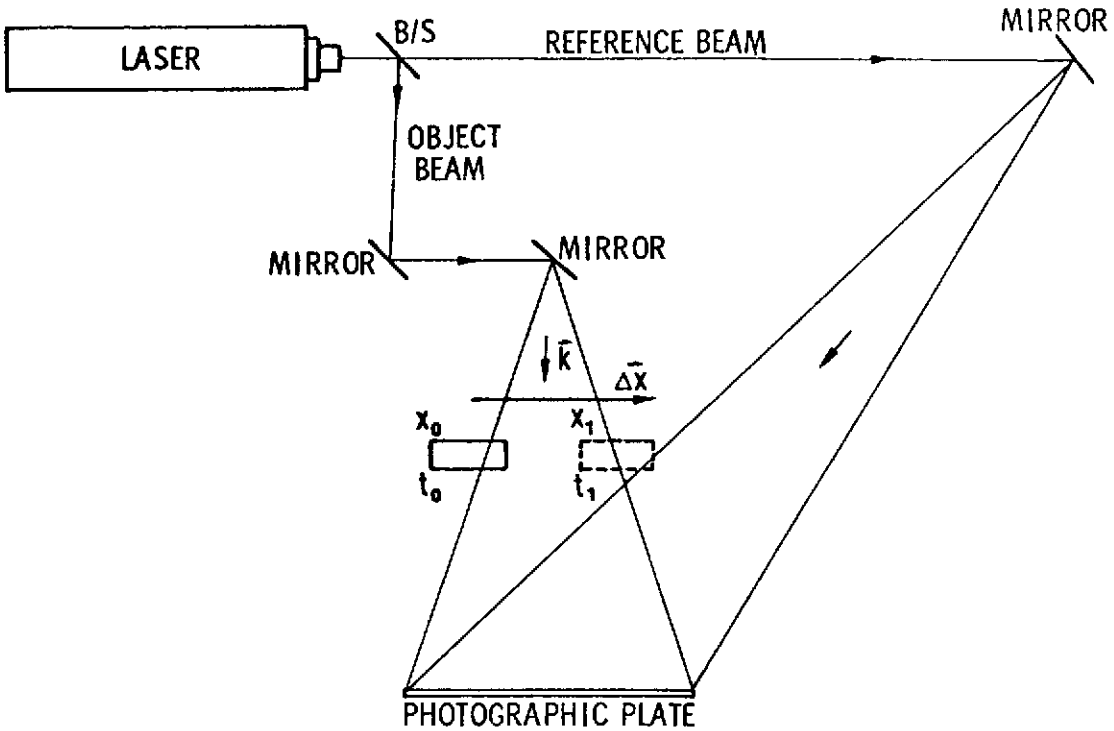

Figure 6. Minimum sensitivity sideband holographic arrangement.

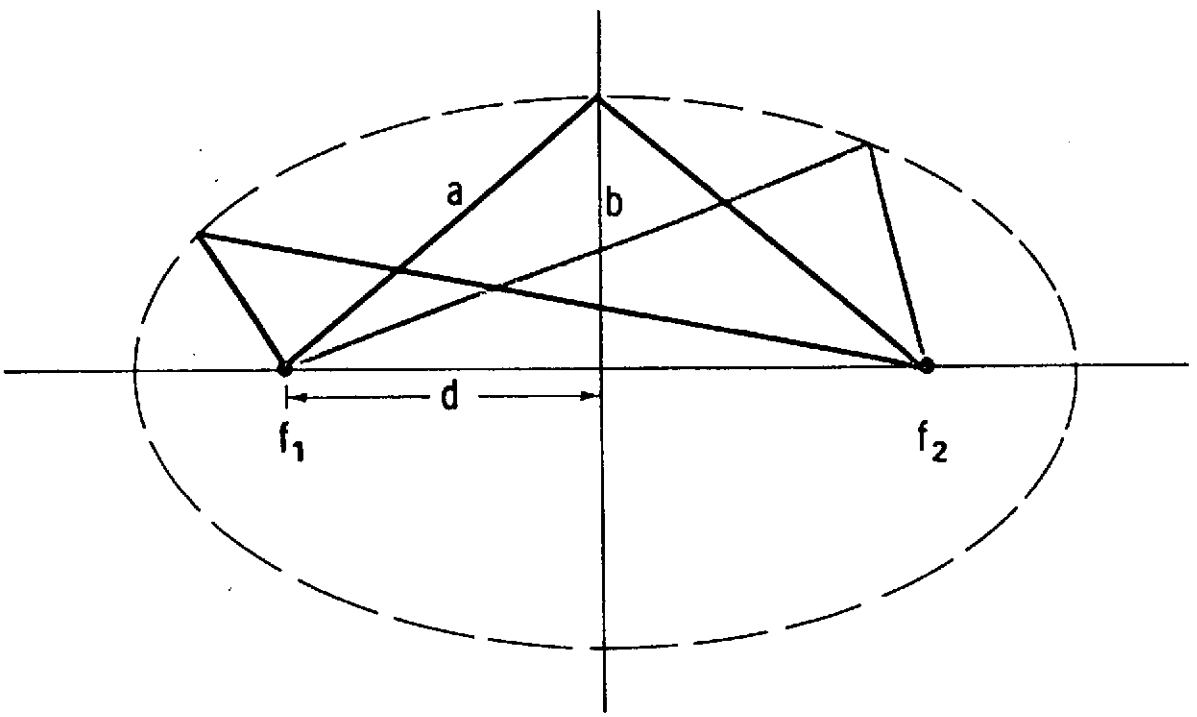

Figure 7. Basic ellipse.

$$\Delta\ell = \left(x_2'^2 + y_2'^2\right)\left(\frac{1}{2}\right)\left(\frac{1}{Z_r} - \frac{1}{Z_1}\right) - x_2'\left(\frac{x_r}{Z_r} - \frac{x_1}{Z_1}\right) - y_2'\left(\frac{y_r}{Z_r} - \frac{y_1}{Z_1}\right), \tag{34}$$

where the numerical subscripts 1 and 2 refer to the subject plane and hologram plane, respectively, and the subscript r refers to some arbitrary reference plane in the reference beam, a distance Z_r from the hologram plane.

Substitution of equation (33) into equation (34) yields the general expression for a circle whose center has the coordinates

$$x_2' = \frac{Z_1\, x_r - Z_r\, x_1}{Z_1 - Z_r} \qquad \text{and} \qquad y_2' = \frac{Z_1\, y_r - Z_r\, y_1}{Z_1 - Z_r} \tag{35}$$

and whose radius P is given by

$$P^2 = \left(\frac{Z_1\, x_r - Z_r\, x_1}{Z_1 - Z_r}\right)^2 + \left(\frac{Z_1\, y_r - Z_r\, y_1}{Z_1 - Z_r}\right)^2 + \left(\frac{Z_n\, Z_1\, Z_1\, Z_r}{Z_1 - Z_r}\right)^2 . \tag{36}$$

An acute sideband holographic system will be discussed later. Provided here is a discussion of just what the effect of such an acute angle means with regard to the interference pattern recorded.

Consider Figure 8, which shows an off-axis intensity pattern formed by the interference of an axial plane reference wave ($x_r = y_r = 0$, $Z_r = \infty$), with a spherical subject (i.e., object) wave diverging from an off-axis point (x, y = 0, Z). The center of the set of circular fringes, whose radii correspond to integral values of n in equation (36), is given by equation (35) as $x_2' = x_1$ and $y_2' = 0$. The result is a zone plate pattern centered at the foot of the perpendicular dropped from P to the plane of the hologram. From Figure 8, if the photographic plate is centered at zero so that it can record only off-center portions of the interference pattern, a sideband hologram is obtained. If θ_1 of this figure is zero, the in-line situation results. For θ_1 equal to a small acute angle, the acute sideband holographic system is formed. The fringe frequency ξ' in the x_2' direction can be found by differentiation of $\Delta\ell/\lambda$ of equations (33) and (34) combined, under the conditions $x_r = y_r = y_1 = 0$ and $Z_r = \infty$. The result is

$$\xi_s' = \frac{1}{Z_1\, \lambda_1}\,(x_1 - x_2') \tag{37}$$

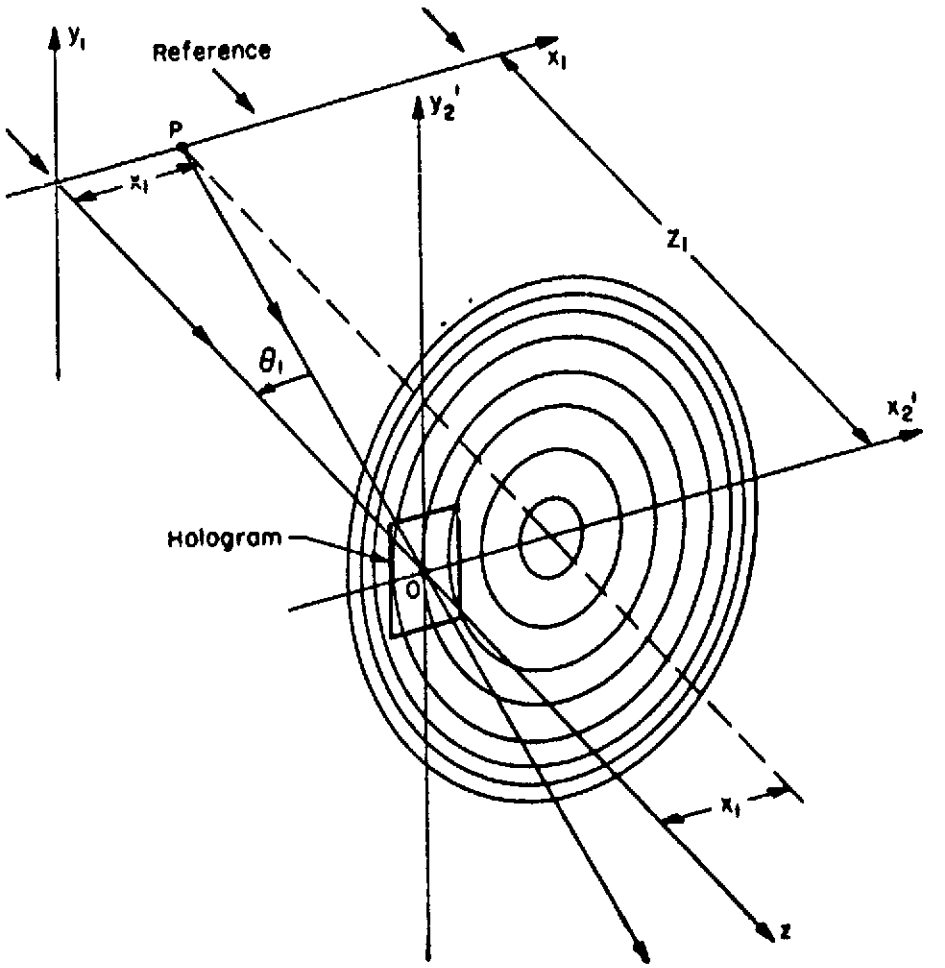

Figure 8. Holographic zone plate produced by off-axis object P.

For the in-line arrangement, the fringe frequency from Reference 11 is given as

$$\xi_i' = \frac{-x_2'}{Z_1 \lambda_1} \qquad (38)$$

As before, assuming the hologram plate to be centered at zero, a comparison of the fringe frequencies for the two arrangements may be accomplished. At the hologram center ($x_2' = 0$), the in-line fringe frequency is zero, while the off-axis fringe frequency is

$x_1/Z_1\lambda_1$. As one proceeds outward in the negative x_2' direction (Fig. 8), the frequency of each fringe system increases linearly with x_2' and this frequency difference is maintained. At the edge of the hologram are generated the highest frequencies to be recorded. If the photosensitive medium on the hologram plate is to record the fringes in the off-axis case, it must have a resolution capability $x_1/Z_1\lambda_1$ in addition to that required for the in-line case. An examination of equation (34) reveals that if an off-axis plane wave were considered ($x_r \neq 0$, $x_r/Z_r = \tan\theta_r \approx \theta_r$), the frequency difference would be

$$\frac{1}{\lambda_1}\left(\frac{x_1}{Z_1} - \frac{x_r}{Z_r}\right) \approx \frac{\theta_1 - \theta_r}{\lambda_1} \quad , \tag{39}$$

where θ_1 is the mean angle to the axis made by the subject wave, i.e., the angle to the z-axis made by a ray passing from P to the center of the hologram at 0. Thus, the mean angle between subject and reference beam provides the difference in the maximum fringe frequency generated in an off-axis hologram compared with the in-line hologram.

In the practical case of an extended subject, either the width of the subject or that of the recording plate can cause the fringe frequency ξ' to exceed the plate resolution R . When the plate is small compared with the subject, then the term $x_1/Z_1\lambda_1$ or $\theta_1 - \theta_r/\lambda_1$ is dominant. Point sources at the extreme dimension of the subject produce the maximum fringe frequency at the plate. If $\xi' > R$ for the extreme portions of the subject, then such portions are not recorded. On the other hand, when the plate is much larger than the subject, the dominant term in equation (37) might be the first. Beyond some value of x_2' all subject points produce zone plate fringes whose frequency $\xi' > R$. That value of x_2' defines the practical extent of the hologram record.

Limited recorder resolution will now be discussed because of its importance to the problem at hand. Consider the x-z plane of Figure 9, where a subject, a reference point source $R(x_r, 0, -Z_r)$, and a recording plate are indicated. The plane normal to the axis and containing the reference point source is separated from the recording plate by the axial distance Z_r . As indicated in Figure 9, a ray from the reference source to an arbitrary point $Q(x_2, 0, 0)$ on the plate makes an angle θ_r with the normal to the plate (the z-axis) and is, therefore, characterized by the spatial frequency ξ_r. Suppose that a small bundle of reference rays interferes in the vicinity of Q with a corresponding bundle of rays from the subject making an angle θ_0 with the z-axis and characterized by a spatial frequency ξ_0. The interference pattern intensity which must be recorded is

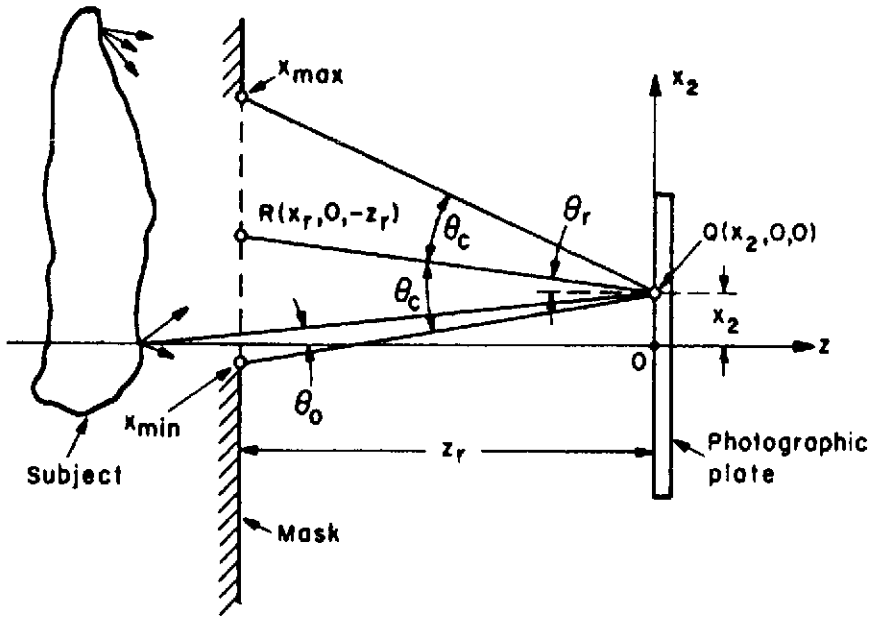

Figure 9. Recorder resolution geometry.

$$I = \left[\exp(2\pi i \xi_0 x_2) + \exp(2\pi i \xi_r x_2)\right]$$

$$\cdot\left[\exp(-2\pi i \xi_0 x_2) + \exp(-2\pi i \xi_r x_2)\right]$$

$$= 2 + 2\cos\left[2\pi(\xi_0 - \xi_r) x_2\right] \quad , \tag{40}$$

where unit amplitude waves have been assumed and the fringe frequency is $(\xi_0 - \xi_r)$. For small angles,

$$\xi_0 - \xi_r = \frac{\sin\theta_0 - \sin\theta_r}{\lambda} \approx \frac{\theta_0 - \theta_r}{\lambda} \quad . \tag{41}$$

Suppose now that the recording medium is perfectly capable of recording all fringe frequencies below a cutoff frequency, ξ_c, but is totally incapable of recording fringe frequencies exceeding ξ_c. For a fixed value of ξ_r and a subject which scatters light over a broad band of spatial frequencies ξ_0, there will be limits to the subject spatial frequencies that can be stored in the hologram; that is, if rays from the subject are to be stored in the hologram, their angles with the z-axis must lie within certain limits. In Figure 9, one such limiting ray passing from the subject to an arbitrary point Q on the hologram plane intersects the plane of the reference source at the point x_{max}. We call this ray a marginal ray, and its spatial frequency $\xi_{0,max}$ satisfies

$$\xi_{0,max} - \xi_r = \xi_c \quad . \tag{42}$$

If the angle the marginal ray makes with the z-axis is $\theta_{0,max}$, then from equation (41),

$$\frac{\theta_{0,max} - \theta_r}{\lambda} \approx \xi_c = \frac{\theta_c}{\lambda} \tag{43}$$

or

$$\theta_{0,max} - \theta_r \approx \theta_c \quad . \tag{44}$$

From Figure 9, the point x_{max} can be obtained and is given by

$$\frac{x_{max} - x_2}{Z_r} = \tan(\theta_r - \theta_c) \approx \theta_r + \theta_c$$

$$\approx \frac{x_r - x_2}{Z_r} + \xi_c \lambda$$

or

$$x_{max} \approx x_r + Z_r \lambda \xi_c \quad . \tag{45}$$

Likewise, for x_{min}

$$x_{min} \approx x_r - Z_r \lambda \xi_c \tag{46}$$

Note that the marginal rays intersect the plane of the reference source at a coordinate independent of the point Q in the recording plane. Note also that if the recording material will not record spatial frequencies greater than $|\xi_c|_2$ (the absolute value of the cutoff frequency), the resolution in the image is limited accordingly. This will be of utmost importance in choosing the best film recorder.

ANALYTICAL DESCRIPTION OF THE ELLIPTICAL HOLOGRAPHIC ARRANGEMENT

The system to be presently discussed provides the basic system which, when modified, will furnish the technique for use as a real-time measurement system for the Zero-g Atmospheric Cloud Physics Laboratory investigations of moving particle fields.

Basic System Description

The elliptical technique is so called because of the relative location of the various optical components with respect to each other. Depending on the magnitude of the expected object motion, a very specific set of locations for the optical components is chosen (i.e., a very specific elliptical arrangement). Further, depending on the direction of the object motion, a very precise orientation of this elliptical arrangement is chosen with respect to this motion vector.

The specific orientation of the holographic system just referred to is based on the use of the specific elliptical holographic arrangement oriented with its major axis parallel to the motion vector defined by the moving object. This motion vector must be made tangent to the mathematical surface of the specific ellipse at some point Q. A typical configuration of this holographic system positioned in the preferred orientation is shown in Figure 10.

This unique system is defined by the following conditions: a thin film beam splitter (B/S) centered at the focus, f_1, of the chosen ellipse; a film recorder centered at the other focus, f_2; and the major axis of this ellipse, defined by xx′ in Figure 10, being parallel to the tangent line, PP′, which is identified as the motion vector of the high-speed particle or object. Laser radiation is incident on the thin film beam splitter, centered at focus f_1. The transmitted beam from here is made incident on the object or particle which is translating linearly along the tangent line, PP′, and is momentarily at

the point, Q, on the perpendicular bisector of xx' at a distance, b, from the major axis, where b is the value of the semiminor axis for the chosen ellipse. This object beam is then made incident on the film positioned at the focus, f_2 . The beam reflected from the beam splitter at f_1 constitutes the reference beam for the system and, after a reflection from a mirror, is made incident on the film at focus f_2. These two beams interfere at f_2 , and the hologram is recorded. Because of the judicious choice of paths for these two beams, their path lengths are matched, and maximum utilization of available coherence length is accomplished.

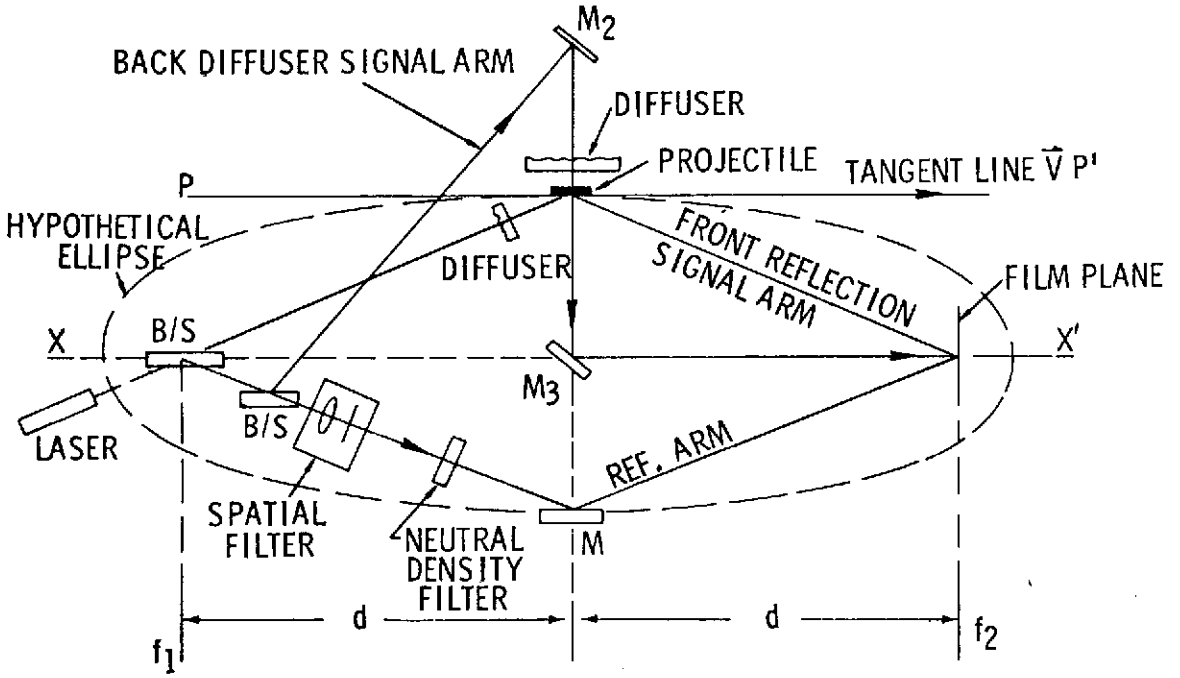

Figure 10. Typical elliptical holographic configuration.

Linear Motion of Object in Terms of Parameters of the Ellipse

Consider Figure 11a; the general equation of such an ellipse is given by

$$b^2 x^2 + a^2 y^2 = a^2 b^2 \qquad (47)$$

The line segment, PP' , is considered to be tangent to this ellipse at the point Q, which lies on the perpendicular bisector of xx' . This line, PP' , in Figure 11a is identical to the tangent line, PP' , of Figure 10. It is the so-called line of motion of the high-speed object,

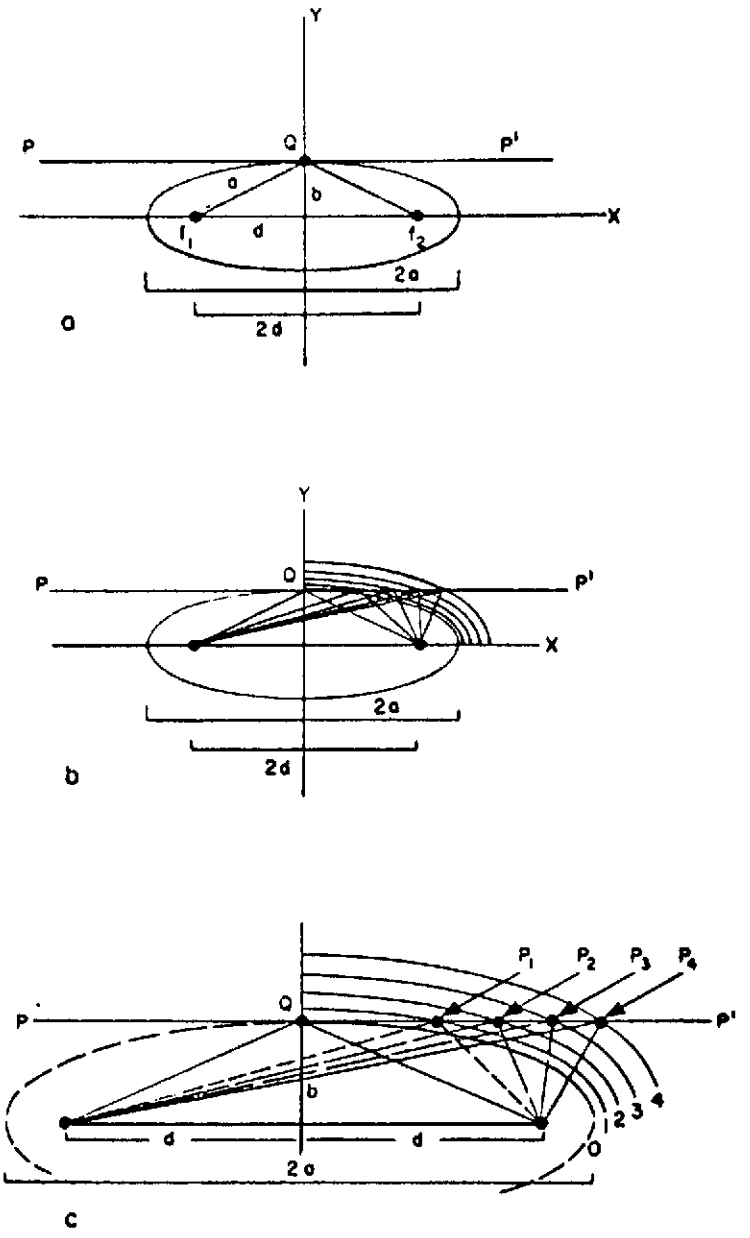

Figure 11. Family of ellipses.

is parallel to the major axis, xx' , of the ellipse, and may be considered perfectly straight. The projectile travels along PP' of Figure 11a and reaches point Q at some time t_0 . The radiation incident at this point at t_0 will be reflected to the film, which is positioned at focus f_2 . At this particular moment the mathematical ellipse passes through point Q, with a beam splitter at f_1 and a film at f_2 , and results in the situation depicted earlier in Figure 10.

As the object moves some incremental distance, Δx , along PP' , past point Q, it moves off this initial ellipse, but it can be considered to move immediately onto another ellipse just slightly larger than the initial one. If the elliptical constant of the initial ellipse was 2a, then the elliptical constant of this new ellipse will be $2(a + \Delta a)$. The radiation reflected from this moving object will then be incident on the film at f_2 and will interfere there with the reference beam, as long as $2\Delta a$ is less than $\lambda/2$.

In Figure 11b a family of such ellipses is constructed, each successive ellipse being intercepted by the line segment, PP' , as one moves from Q to the right along PP' parallel to the x-axis of the coordinate system. The separation of the foci must remain constant and equal to 2d for the entire family of curves. Figure 11c is a convenient enlargement of the first quadrant of Figure 11b. The points of interception of PP' with each successive member of the family of ellipses are given by P_1, P_2, P_3, etc., respectively. As PP' is traversed to the right, the original ellipse can be considered to grow successively to the next larger member of its family, while the foci separation distance 2d remains constant.

If one considers that the ellipse is to enlarge during the time t, then expanding to a larger ellipse, equation (47) becomes

$$b^2 x \Delta x + b \Delta b x^2 + a^2 y \Delta y + a \Delta a y^2 = a^2 b \Delta b + b^2 a \Delta a \quad . \quad (48)$$

Since the direction of object motion is parallel to the x-axis, $\Delta y \equiv 0$ and

$$b^2 x \Delta x = a \Delta a (b^2 - y^2) + b \Delta b (a^2 - x^2) \quad . \quad (49)$$

However, from Figure 10a,

$$a^2 - b^2 = d^2 \quad , \quad (50)$$

where d is a constant; therefore,

$$a \Delta a = b \Delta b \quad ,$$

and equation (49) becomes

$$b^2 x \Delta x = a \Delta a [a^2 + b^2 - (x^2 + y^2)] \quad . \quad (51)$$

From the basic equation for the ellipse, equation (47), one may easily obtain

$$x^2 + y^2 = b^2 + x^2 [1 - (b^2/a^2)] \quad . \tag{52}$$

Substituting equation (52) into equation (51) gives

$$x \Delta x = (\Delta a/ab^2) (a^4 - d^2 x^2) \quad . \tag{53}$$

For any ellipse, $2a = L$, where L is a constant and at present is the optical path length of the front illumination signal arm. When the ellipse expands as a result of object travel along PP', then $2a = L$ changes by $2\Delta a = \Delta L$. Therefore, since $\Delta a = \Delta L/2$, equation (52) becomes

$$x \Delta x = (\Delta L/2) (1/ab^2) (a^4 - d^2 x^2) \quad . \tag{54}$$

Now since point Q has been taken as the reference point for x (i.e., x is zero when the projectile is at point Q), as measurement of the projectile motion starts from point Q and traverses to some point P, $x = \Delta x$ and equation (54) becomes

$$(\Delta x)^2 = (\Delta L/2) (1/ab^2) [a^4 - d^2 (\Delta x)^2] \tag{55}$$

or

$$(\Delta x)^2 = \frac{\Delta L \, a^3/2b^2}{1 - (\Delta L d^2/2ab^2)} \quad . \tag{56}$$

Making the assumption that the magnitude of d^2 is not drastically different from b^2 and $\Delta L/2 << a$,

$$\Delta L \, d^2/2ab^2 << 1$$

and equation (56) becomes

$$(\Delta x)^2 \simeq (\Delta L/2) (a^3/b^2) \quad , \tag{57}$$

where $\Delta L = 2\Delta a$ is the variation in the original elliptic constant 2a resulting from the travel of Δx of the object along PP′. At a given velocity V for a time t,

$$\Delta x = Vt \quad , \tag{58}$$

where t is the pulse length and also the exposure time.

Equation (57) is, therefore, an expression which relates the distance Δx traveled by the object along PP′ to the total change in the elliptic constant, $\Delta L = 2\Delta a$; i.e., ΔL is the change in the optical path length of the front-surface illumination arm of the holographic system. Substituting equation (58) into equation (57) and solving for the object velocity,

$$V = (\Delta L/2)^{1/2}\, a^{3/2}/bt \quad . \tag{59}$$

This relation may be used to determine the permissible object velocities allowed by the specific configuration having a set of elliptic parameters and a specified tolerance ΔL. For illustration, one may arbitrarily set ΔL equal to $\lambda/8[\lambda = 694.3$ nm (6943 Å)] and let the distance of separation between the center of the first beam splitter, at f_1, and the center of the photographic film, at f_2, be a constant value 2d. By varying the semimajor axis a, which in turn varies the semiminor axis b, a set of permissible velocities can be obtained. This set of velocities is graphically shown in Figure 12, where the permissible velocity values have been used as the ordinate and the arbitrarily chosen values of the semimajor axis a as the abscissa. Each separate curve corresponds to a specific value of d, and the elliptic parameters are related by $a^2 = d^2 + b^2$.

It may be interesting to note the following three items. First, for this fixed value of ΔL and each assigned value of d, the curve approaches the vertical line, a = d, asymptotically. This seems to indicate that the projectile velocity can be any high value without limit if a = d. Obviously this is not practical since at a = d, b = 0, and the object would have to pass directly through the beam splitter and film. However, picking the smallest practical value of b allows the highest possible velocity for a given value of d. As the assigned value of d increases (bounded by some practical value of d), the curve rises and thereby raises the allowed value of velocity. However, because of the steepness of the curve, this region may be somewhat unstable with respect to changes in a or b.

Second, as the assigned value of d decreases, the respective curve lowers. The lower bound for these curves occurs at d equal to zero, i.e., the mathematical ellipse becomes a circle. This is again impractical because the beam splitter would be located at the photographic plate.

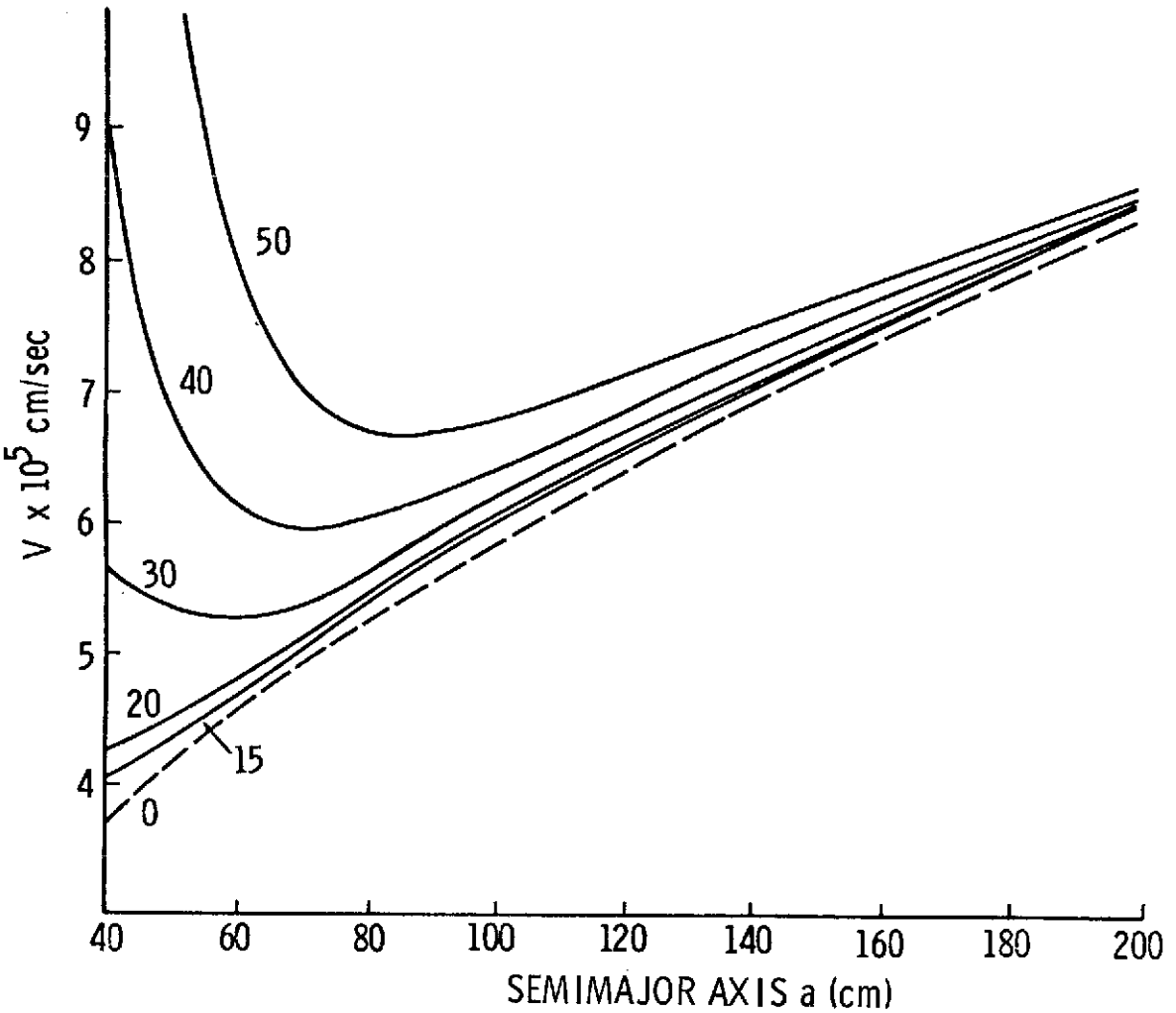

Figure 12. Graph of permissible velocities vs parameters of ellipses.

Third, the differentiation of equation (59) shows that each curve has a minimum at the value of $a = \sqrt{3}d$. Substitution of this back into equation (59) produces

$$V_{min} = (3^{3/4}/2)\,(d\,\Delta L/t^2)^{1/2} \quad . \tag{60}$$

This V_{min} is the minimum permissible value of the velocity for each specific value of d. Because each curve has a zero slope at this point, the region about this point is the most stable region with regard to possible changes in the values of the elliptic

parameters a or b. (Changes in a, and therefore b, will occur as the mathematical ellipse enlarges because of object travel Δx; further changes in b, and therefore a, might occur because of the projectile varying slightly off path as it travels along the line of motion.) Because of this stability, this region probably constitutes the best choice for an actual experiment.

In view of the constant consideration given to the direction necessary for the velocity vector for this system and the stated fact that this velocity vector must be parallel to the major axis of the chosen ellipse, it remains now to discuss the total depth of volume allowed by this system.

An experimental and theoretical discussion of the allowed volume is presented in References 5, 6, and 11, where it is shown that the allowed volume is a function of the total displacement of the object during the exposure, Δx, and the parameters a, b, and d for the chosen ellipse; i.e.,

$$\text{Vol} = f(a, b, d, \Delta x) \quad .$$

It obviously will be a function of the total volume originally illuminated since the enlarging or spreading of the illumination beam allows the system to function over a family of chosen ellipses instead of just one. This is explained by the fact that each separate angle formed by an enlarged or spreadout beam selects a separate member of the family of chosen ellipses.

Consideration of the Primary Parameter of Motion Holography — Total Motion of the Object Field During Exposure

The parameter of importance to motion holography is neither the velocity of the object, V, nor the exposure time, τ, by itself. Rather, it is the constant product of these two parameters, which is the total distance, Δx, traveled by the object during the exposure time; i.e.,

$$\Delta x = V\tau \quad . \tag{61}$$

This obvious statement has been reiterated for clarity, and Figure 13 is presented as a more useful engineering diagram for employment in developing the acute sideband holography technique described later. This figure is only a modified version of Figure 12 and may be used to determine the feasibility of obtaining a hologram of a particle traveling at 6.096×10^5 cm/sec (20 000 ft/sec).

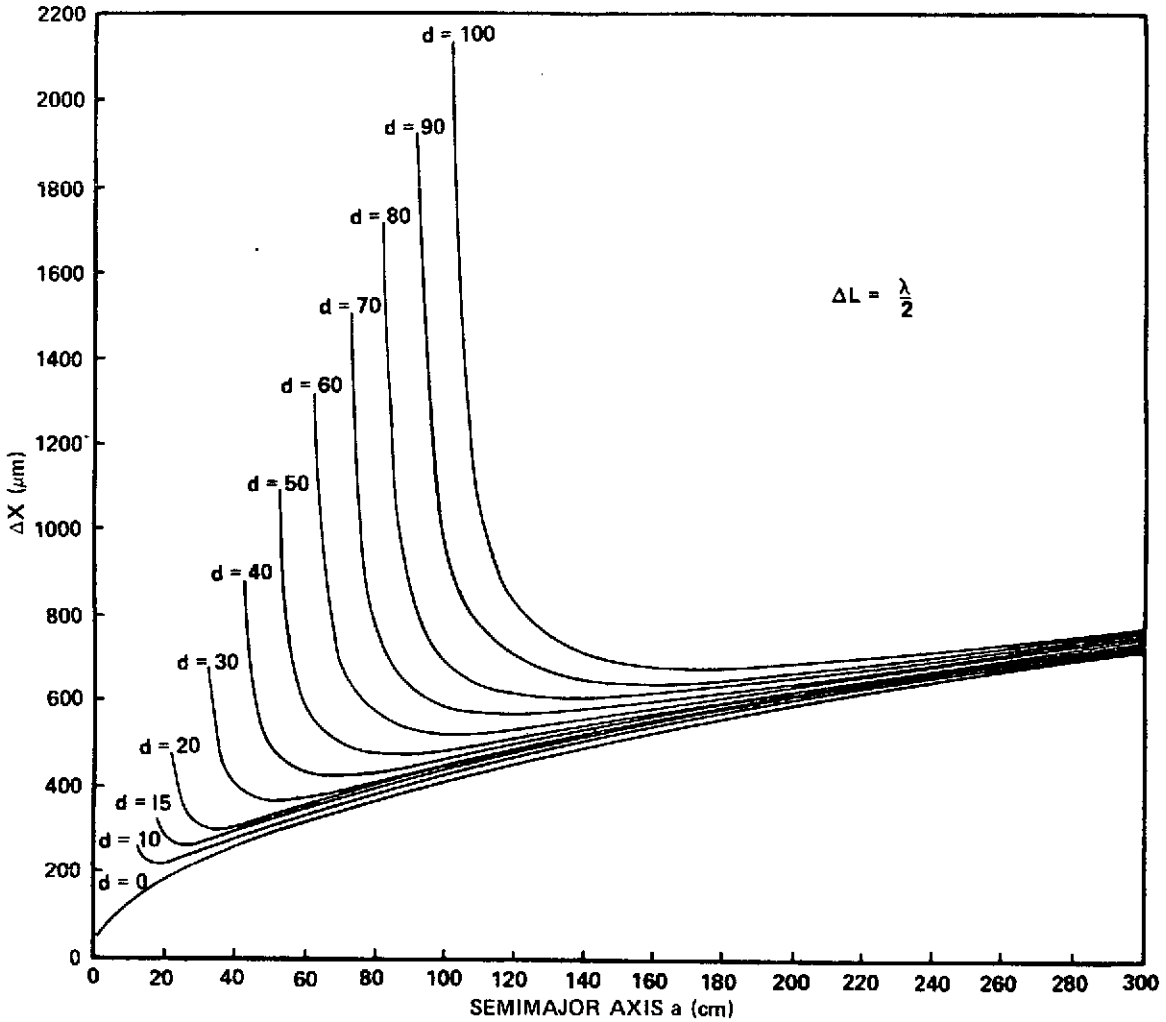

Figure 13. Engineering diagram for determination of permissible object motion.

From the experimental evidence of References 5 and 9, the value of total particle travel, Δx, during the exposure is allowed to be 700 μm for a successful hologram. Using this value for Δx, Figure 13 indicates that an ellipse with a value of 50 cm for d will suffice. Then for any ellipse,

$$a^2 = d^2 + b^2 \quad , \tag{62}$$

and, depending on the geometry, a value of b as small as is practical is selected. Equation (62) provides the magnitude for the semimajor axis a. A specific ellipse has now been chosen by first obtaining an expected Δx which allows a successful hologram.

One must now use Δx and the expected particle velocity to obtain an exposure time or pulse length and then decide if this exposure time is realistic or feasible; if so, then the chosen holographic system is feasible. Consider that

$$\Delta x = 700 \times 10^{-4} \text{ cm}$$

and

$$v = 20\,000 \text{ ft/sec} = 6.096 \times 10^{5} \text{ cm/sec} \quad ;$$

then

$$\tau = \frac{\Delta x}{v} = 114 \times 10^{-9} \text{ sec}$$

and

$$\tau = 100 \text{ nsec} \tag{63}$$

Therefore, this chosen system would be feasible with a ruby or pulsed argon laser as a source.

BASIC DESIGN OF THE OPTICAL HOLOGRAPHIC TECHNIQUE PROPOSED FOR THE REAL-TIME MEASUREMENT OF THE PARTICLE FIELD GROWTH RATES

The basic design to be used for the laboratory investigation of the various cloud physics chambers will be a modification of the basic elliptical configuration discussed previously. This modified basic design will constitute a laboratory-type system constrained only by the primary parameter of motion holography – the total motion of the particle field during the exposure and the resolution limit of the system.

Consider Figure 14, which shows the modified basic elliptical technique (acute sideband). Based on the information of Figure 13, the parameters for this ellipse are given by

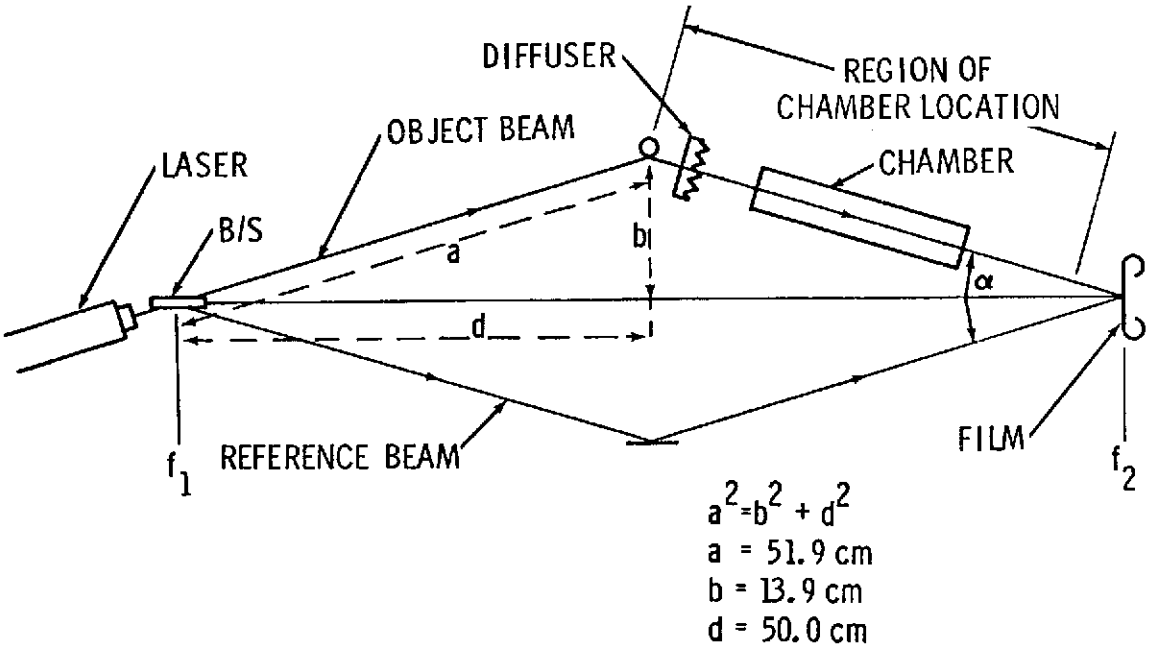

Figure 14. Modified basic elliptical technique.

semimajor axis, a = 51.9 cm,

semiminor axis, b = 13.9 cm,

and (64)

foci-origin separation, d = 50 cm .

Now from a combination of equations (58) and (59), an expression for the allowable total travel, Δx, is

$$\Delta x = \left(\frac{\Delta L}{2}\right)^{1/2} \cdot \frac{a^{3/2}}{b} \tag{65}$$

Now consider the quantity

$$\Delta L = 2\,\Delta a \quad , \tag{66}$$

which is the total change in the optical path length of the front-surface illumination arm (object beam) caused by the total motion of the object during the exposure. This quantity, ΔL, must be less than $\lambda/2$ for a successful hologram. The value

$$\Delta L = \lambda/4 \tag{67}$$

is chosen because this should be a good reconstruction of the moving particle.

Substituting the values from equations (64) and (67) into equation (65) allows the calculation of the total expected travel, Δx, permitted by this system.

$$\Delta x = \left(\frac{\lambda}{4} \frac{1}{2} \right)^{1/2} \frac{(51.9 \text{ cm})^{3/2}}{13.9 \text{ cm}} \tag{68}$$

and λ for an argon laser is 5145×10^{-8} cm; therefore,

$$\Delta x = \left(\frac{5145 \times 10^{-8} \text{ cm}}{8} \right)^{1/2} \frac{(51.9 \text{ cm})^{3/2}}{13.9 \text{ cm}}$$

$$= \frac{(25.359 \times 10^{-4} \text{ cm}^{1/2})(373.896 \text{ cm}^{3/2})}{13.9 \text{ cm}} \tag{69}$$

$$\Delta x = 682.132 \times 10^{-4} \text{ cm}$$

Consider now a shutter speed of 1/60 sec commensurate with the 10 fps of the Hulcher 70 film transport. Then the useable pulse length is

$$\tau = 17 \text{ msec} \quad , \tag{70}$$

$$\tau = 17 \times 10^{-3} \text{ sec}$$

Using

$$\frac{\Delta x}{\tau} = V \quad , \tag{71}$$

$$v = (682 \times 10^{-4} \text{ cm})/(17 \times 10^{-3} \text{ sec}) \quad ,$$

$$v = 40 \times 10^{-1} \text{ cm/sec} \quad , \tag{72}$$

$$v = 4 \text{ cm/sec} \quad .$$

The exposure time of 1/60 sec represents the longest exposure time even anticipated. Consider now the shortest exposure time which is readily available,

$$\tau = 25 \times 10^{-9} \text{ sec.}$$

With this exposure time the allowable velocity becomes

$$v > 31.696 \times 10^{9} \text{ cm/sec} \quad ,$$

$$v \approx 21\,000 \text{ mph} \quad . \tag{73}$$

Primary Constraints on Prototype System

As mentioned, the primary constraints on the prototype system will be total motion during exposure and resolution limit. From equation (69) the total motion of 682 μm is obviously more than adequate when recorded with the proper exposure time.

The second constraint of resolution limit appears to be a more limiting one in view of the requirement of the smallest particle sizes to be observed in the zero-g atmospheric cloud physics chambers. The desired range on the particle diameters, P_D, of these chambers is

$$0.01 \ \mu\text{m} \leqslant P_D \leqslant 10\,000 \ \mu\text{m} \quad . \tag{74}$$

Since this range covers six orders of magnitude, no single system could be expected to monitor the entire range. The proposed technique, however, appears to be able to cover four orders of magnitude,

$$1\ \mu m \lesssim P_D \leqslant 10\,000\ \mu m \quad , \tag{75}$$

and still be able to reconstruct an image. Using basically the same system but reading the data in a different fashion, it is conceivable that the other two orders of magnitude could be obtained; i.e.,

$$0.01\ \mu m \leqslant P_D \leqslant 1\ \mu m \quad . \tag{76}$$

The details of this will be covered in the next section.

Analytical and Experimental Testing of Primary Constraints and Indication of System Response

With regard to the primary constraint of total motion during the exposure of the hologram, there appears to be no problem as long as this motion is approximately 500 to 700 μm. This total motion can always be controlled in the present situation of the cloud physics chambers by proper control of the pulse length or exposure time of the laser source.

Several tests have already been performed in an effort to ascertain the total allowed motion. Figure 15 displays the experimental arrangement in which the free-fall motion of calibrated glass bead particles was used. Using the total allowed motion of 700 μm and $g = 980\ cm/sec^2$, the exposure time was properly adjusted and the spherical, calibrated particles were successfully recorded.

Using the same system as shown in Figure 15, the hopper and calibrated particles were replaced by a water chamber (Fig. 16). Air was constantly fed into this water tank, and the rising bubbles of varying size were recorded. Figure 17 displays the results from this experiment. The chamber and bubbles were recorded with a lens interposed between the chamber and the film for prerecorded magnification (Fig. 17a) and without lens magnification (Fig. 17b).

With this system and premagnification, particles in the range of from 1 to 3 μm may be recorded and imaged. The relation between recording distance and particle size for this system was established by using various arrays of particles and a high-resolution test target.

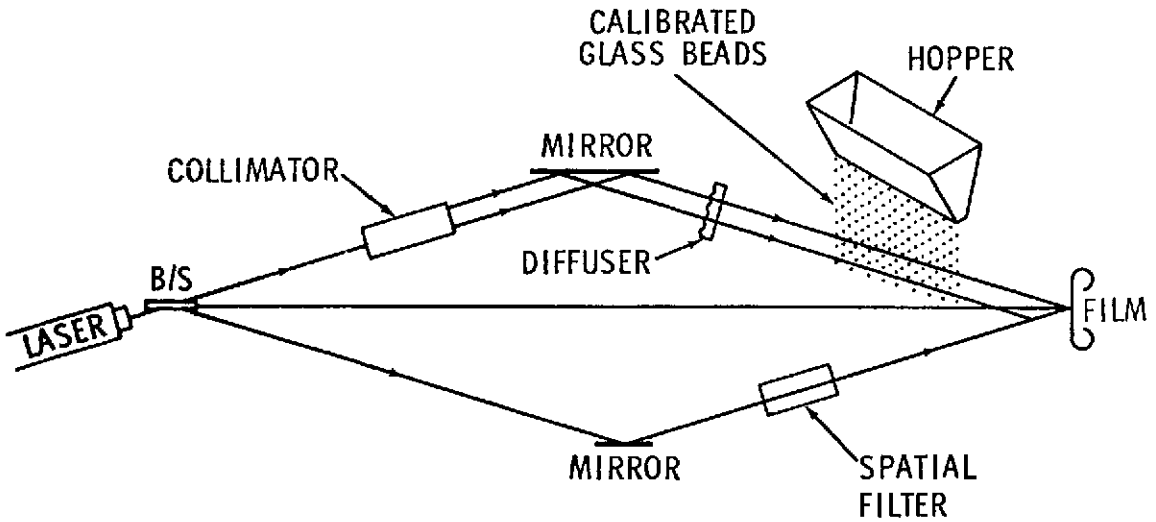

Figure 15. Experimental arrangement for holography of free-fall objects.

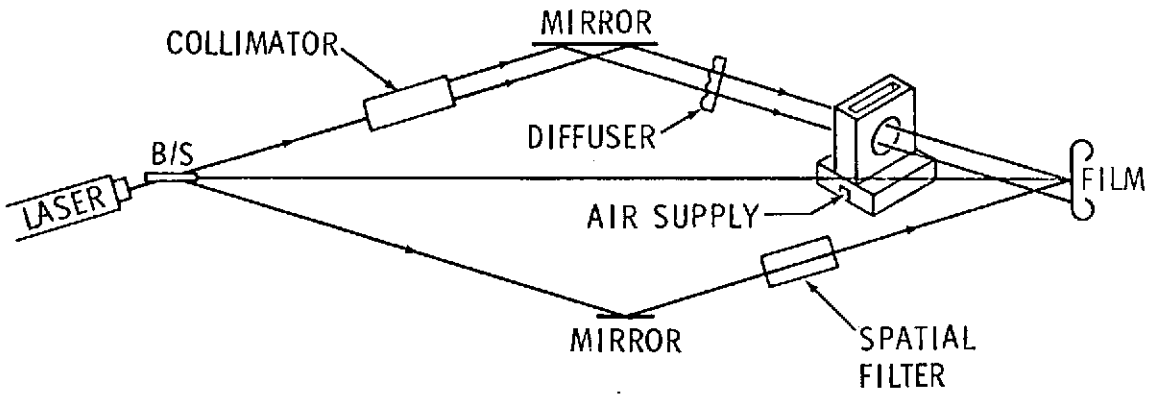

Figure 16. Experimental arrangement using water chamber.

Figure 18 presents this graphical relation. Figure 19 displays a photograph of the virtual image of the high-resolution test target using premagnification. The resolved line in the lower right-hand corner is 251.2 lines/mm, which is roughly equivalent to the resolution of a 3-μm particle.

These rough tests have been only for the basic response of the system. The intentions are to properly refine these techniques, apply both pre- and post-magnification, and automate the reading and detection techniques. Further intentions are to use the various cloud physics chambers for real-time detection of the existing particles.

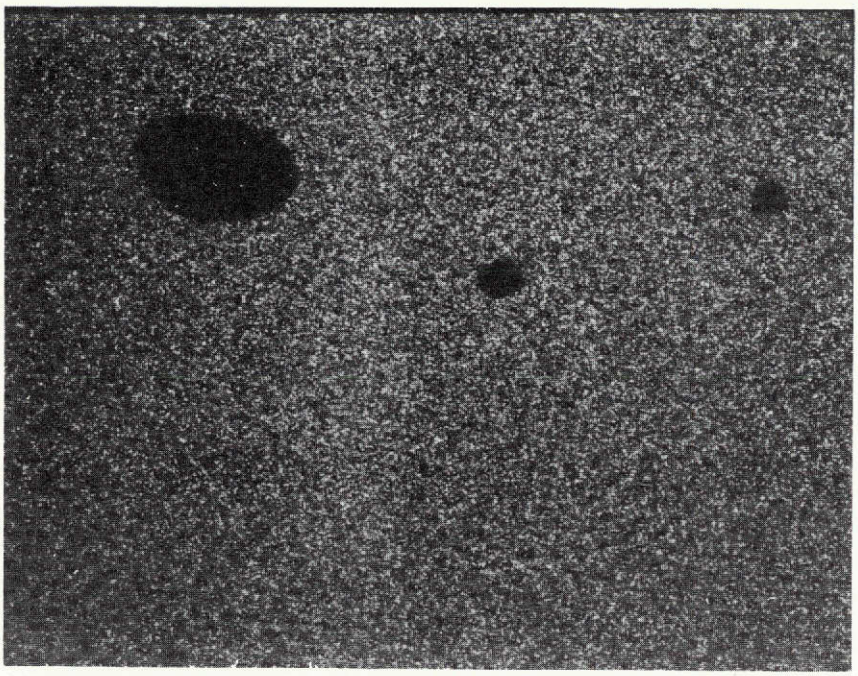

a. With lens magnification.

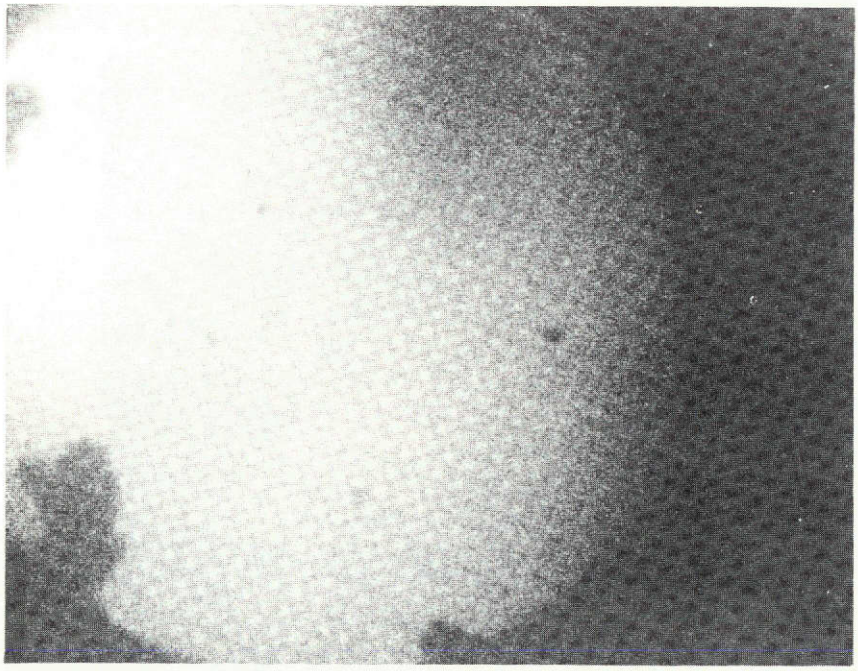

b. Without lens magnification.

Figure 17. Experimental results using water chamber.

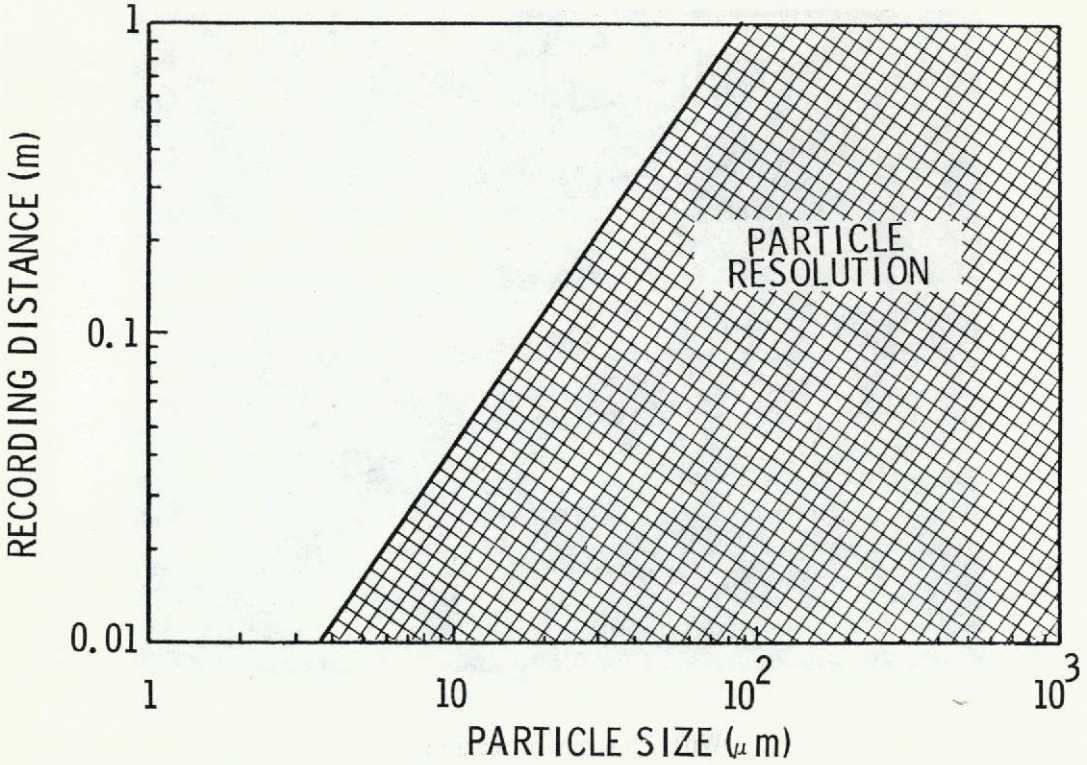

Figure 18. Engineering diagram for particle resolution vs recording distance.

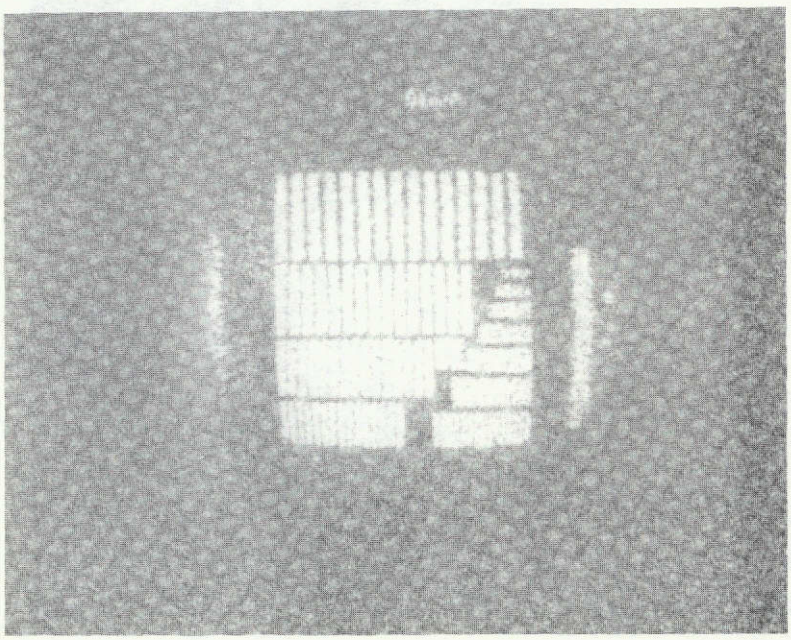

Figure 19. Photograph of high-resolution test chart recorded holographically.

This same system can be employed to detect the lower range of particles, i.e.,

$$0.01\ \mu m \leqslant Pd \leqslant 1\mu m \quad ,$$

if the data are handled in a different fashion.

The image of such a particle is not reconstructed; rather, the hologram is treated as an interferogram. The use of this technique is called submicron holography and may be described as follows. The basic technique is to use the hologram as an interferogram. Then, from the intensity distribution of the diffraction pattern of an individual particle, one determines the radius, r, of the airy disc. This is related to the particle size by

$$2a = \frac{1.22Z\lambda}{r} \quad ,$$

where 2a is the diameter of the particle, and Z is the distance of separation of the particle from the film plane, i.e., object distance. The above equation is, of course, for a particle with a circular cross section. However, for a particle with an arbitrary cross section, one simply considers 2a to be the largest dimension of the particle.

The limitation here is, of course, that there is no image with which to work. Obviously one can get size and size distribution from this information, but any other information would be difficult because one could only monitor the motion of an array of airy discs caused by the presence of the particles. This technique must be investigated further.

CONCLUSIONS AND RECOMMENDATIONS

Four important processes in clouds must be better understood before deliberate weather modifications can occur. These are nucleation, growth, scavenging, and electrical charge separation. This necessary understanding can be greatly facilitated through the Zero-g Atmospheric Cloud Physics program. In the entire study of cloud physics, primary interest is centered on observing various parameters of particles having a wide range of forms and sizes. More importantly, the forms and sizes occur over and within some volume, i.e., the various cloud chambers. Obviously, the simultaneous recording of a depth of particles is to be highly preferred over the recording of a limited planar cross section through this volume. This is the case of holography versus photography (Table 1).

TABLE 1. COMPARISON OF HOLOGRAPHIC AND PHOTOGRAPHIC RECORDINGS

Characteristic	Photographic	Holographic
Cost of Media and Replication	Expensive silver halide media and wet processing required for archival master and hard copies.	Ordinary vinyl tape suitable for a copy medium using hot embossing technique.
Reduction Ratio	Limited by scratches, dust, lens depth of focus (which is inversely proportional to the lens f/no.), and registration requirements of the system.	Relatively immune from scratches; a large effective depth of focus, and relatively tolerant of registration errors.
Brightness of Image for a Projection System	Dependent on the luminance which the film can produce before distorting due to heat and proportional to the lens f/no.	Dependent on source brightness and efficiency of hologram. (A phase medium does not absorb light, i.e., heat.)
Optical Limitations for High Reduction and Display Resolution	1. A large f/no. is required (to satisfy the diffraction limit requirements on the lens) which, for moderately priced lenses, is specified only for a limited field of view and a shallow depth of focus. 2. High-cost lenses required to record and reproduce.	1. Large depth of focus inherent in hologram. 2. Requires lower-quality lens, especially if matched lenses are used to record and reproduce. 3. Field of view limited by resolution of recording medium.
Index Information Registration	Misregistration causes loss of information.	Misregistration causes loss of brightness.

The particles of concern to the cloud physicist fall into two basic categories: the condensation nuclei, which range from 0.01 μm to about 1 μm, and the giant nuclei, which include all particles greater than 1 μm. It has been shown that the entire particle size spectrum is from 0.01 μm to 10 000 μm or 1 cm.

It has also been demonstrated that holography provides an image of the total volume of particles with one exposure. Therefore, holography captures the entire field distribution of particles within the total chamber volume instantaneously with one exposure. However, its resolution is limited to the top two-thirds of the particle size spectrum. Photography, on the other hand, does not have this resolution limitation, but it is severely limited by its inability to record the total volume. It must record only a planar cross section through the chamber.

To properly utilize the advantages of both of these recording techniques, holography should be applied to all cloud physics chambers in the system described earlier. This will provide volumetric data throughout each of the individual chambers with regard to particle growth, trajectory, growth rate, and the other pertinent parameters. Additionally, for information on the particles falling in the lower one-third of the size spectrum, photography should be utilized. The two recording techniques can easily be employed in a hybrid arrangement. This hybrid system could be fashioned similar to the following. Use the modified basic ellipse system discussed earlier for the holographic system. Record the hologram on holographic film using either a 70- or 35-mm film transport. To employ the photography, rotate a turret to properly place the lens system for the camera which will utilize the same film and film transport. The illumination for the photographic camera system would be due to the object beam of the holographic system alone, i.e., use only one of the two beams in the holographic system. To use the holographic camera again, simply rotate the turret again to remove the lens from the object beam, and the holographic system would still record on the same film transport.

Another possibility would be to use a beam splitter to allow both holography and photography to record events in a given chamber simultaneously instead of sequentially, as indicated above. In any case, a hybrid technique such as this would utilize the advantages of both recording techniques without any of the concomitant disadvantages of either.

George C. Marshall Space Flight Center
National Aeronautics and Space Administration
Marshall Space Flight Center, Ala. 35812, Oct. 30, 1973
645-10-01-000

APPENDIX

THEORETICAL DEVELOPMENT OF HOLOGRAPHY

Effect of Linear Scene Motion During Hologram Exposure

The effect of scene motion during the exposure of a hologram is a spatial modulation of the recorded fringe contrast. This, in turn, causes a spatial amplitude modulation of the reconstructed wave front that blurs the reconstructed image in the same way that it would blur a conventional photograph having the same exposure time. In addition, this modulation reduces the brightness of even that part of the image that is reconstructed. The amount of object motion that can be successfully tolerated during the hologram exposure certainly depends upon the geometry of the holographic configuration with respect to the velocity vector of the motion.

Two different theoretical approaches to the time-dependent theory of motion holography will be presented which follow closely the methods presented by Neumann [12]. Both approaches serve a purpose. The first uses a coordinate system with its origin at the scene point of interest, which is a vector approach that allows a more intuitive feeling for the physics of the problem. It is primarily valid only for those cases where the allowed motion is small compared with the distance from the scene to the hologram. The second approach uses a coordinate system with the origin at the hologram. It is the most general derivation, and if a sufficient number of terms are taken in the infinite series that occurs, it will cover all geometries. It suffers, however, from the mathematical complexity that results from these expansions.

Scene-Oriented Coordinates. Following Neumann, a basic holographic configuration is assumed (Fig. A-1). The radiation from the laser is split into two beams. As usual, these are considered to be the reference beam and the signal beam. Let the point R of Figure A-1 serve as the reference position for the system and S be some point of the scene. Light scattered from point S is made incident at the point P of the hologram, where it now interferes with light from the reference point.

Let the field at point P be given by

$$\vec{E}(P) = \vec{E}_r(P) + \vec{E}_S(P)$$

or

$$E(P) = E_r(P)\, e^{i[\omega t - kr(P)]} + E_s(P)\, e^{i[\omega t - ks(P)]} \quad , \qquad \text{(A-1)}$$

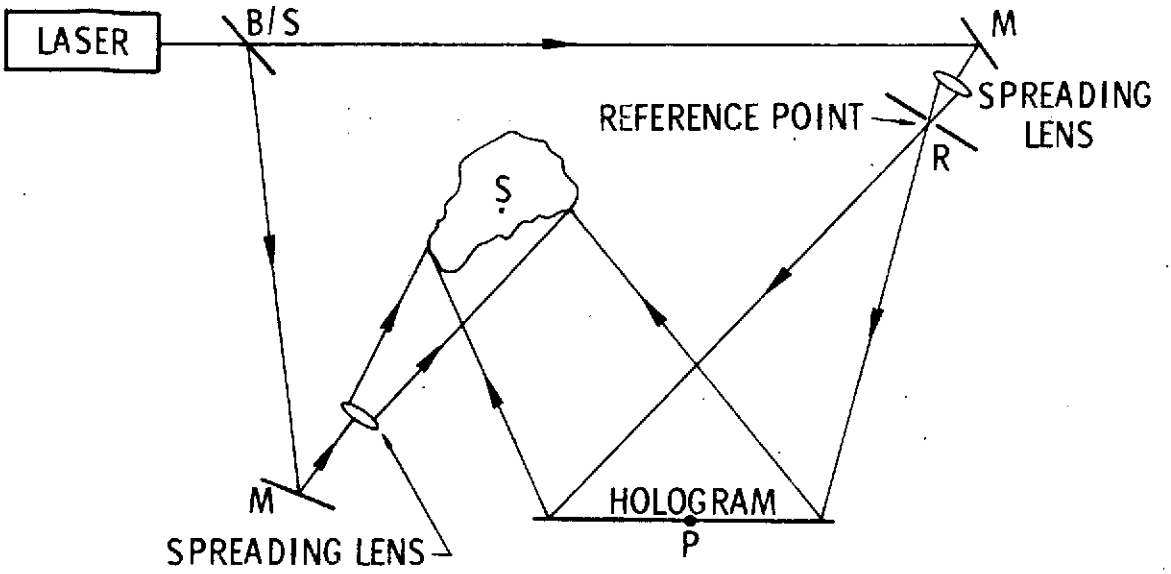

Figure A-1. Typical configuration.

where $\vec{E}_r(P)$ is the contribution from the reference point and is considered to be plane polarized, $\vec{E}_s(P)$ is the contribution at P because of the scene point, S, and is the component of the scene-field parallel to the reference polarization, and r and s are the corresponding path lengths from the laser to the point P.

Now, the intensity is given by

$$I = m\,|E|^2 \quad .$$

Therefore,

$$I = m\,[E_r^2 + E_s^2 + 2E_r\,E_s \cos k(r - s)] \quad . \qquad \text{(A-2)}$$

If the point, S, is allowed to move with some velocity, then s becomes a function of time. It is assumed, however, that the field amplitude does not change appreciably over the time, τ, of the exposure. Thus, the interference pattern remains approximately constant except for the motion of the fringes.

Then, as before, the exposure can be written as

$$\mathcal{E}(P) = m \int_{-\tau/2}^{\tau/2} \left\{ E_r^2 + E_s^2 + 2E_r E_s \cos k[s(t) - r] \right\} dt$$

and

$$\mathcal{E}(P) = m\tau \left\{ E_r^2 + E_s^2 \frac{2E_r E_s}{\tau} \int_{-\tau/2}^{\tau/2} \cos k[s(t) - r] \right\} dt$$

Let

$$K_C = E_r^2 + E_s^2$$

and

$$\mathcal{E}(P) = m\tau \left\{ K_C + \frac{2E_r E_s}{\tau} \int_{-\tau/2}^{\tau/2} \cos k[s(t) - r]\, dt \right\} . \qquad \text{(A-3)}$$

To proceed, the time dependence of s must be given. In general, $s = s_0 + f(t)$ where f(t) may be any function of time where the midpoint of the exposure is at $\tau = 0$.

In particular, if it is assumed that s varies linearly with time, the result is

$$s = s_0 + vt \quad ;$$

then equation (A-3) becomes

$$\mathcal{E}(P) = m\tau \left\{ K_C + \frac{E_r E_s}{\frac{\tau}{2}} \int_{-\tau/2}^{\tau/2} \cos [kvt + k(s_0 - r)]\, dt \right\} . \qquad \text{(A-4)}$$

Let $\Phi = k(s_0 - r)$ be the time-invariant portion; then

$$\mathcal{E}(P) = m\tau \left[K_C + \frac{E_r E_s}{\frac{\tau}{2}} \int_{-\tau/2}^{\tau/2} \cos(kvt + \Phi)\, dt \right] \tag{A-5}$$

after integration:

$$\mathcal{E}(P) = m\tau \left(K_C + E_r E_s \frac{\sin kv\frac{\tau}{2}}{kv\frac{\tau}{2}} \cos\Phi \right) . \tag{A-6}$$

Then, since $\sin x/x = \operatorname{sinc} x$, one obtains for the exposure

$$\mathcal{E}(P) = m\tau \left[K_C + E_r E_s \operatorname{sinc}(kv\,\tau/2) \cos\Phi \right] . \tag{A-7}$$

If $V = 0$, then no motion exists (i.e., the stationary case), and the sinc function becomes unity. This is the most desired case for most holographic experiments, i.e., that the argument of the sinc function be zero.

It is observed that if V is constant over the hologram, the resulting fringe contrast of the exposure will be poor for large values of the sinc argument, and the resulting fringe contrast will be zero whenever the argument is $n\pi (n = \pm 1, 2 \ldots)$. Consider, for example, $n = 1$, where the first zero occurs; then,

$$\frac{kv\tau}{2} = \pi \tag{A-8}$$

or

$$v\tau = \lambda . \tag{A-9}$$

Now, since $v\tau$ is the change in the distance, s, during the exposure, the possibility exists that motions of the scene as small as a wavelength may totally destroy the fringes or, at best, result in a poor hologram. Fortunately, V is not the same for all points of the hologram, and the fringe contrast is spatially modulated rather than destroyed.

This special case of the linear time variation of s has demonstrated the sinc function modulation of the recorded fringes. The problem may now be discussed with respect to the velocity vector of the motion. Consider the diagram in Figure A-2, where R is the reference point and, as before, S is the scene point. Let L be a point on some reference phasc front from the laser, which will be common to both beams. Let $\hat{a}_k$ be the unit vector along the direction of propagation of the incident laser radiation at the scene point, S; $\hat{a}_p$ be a unit vector along the line from scene point, S, to hologram point P; and $\hat{a}_v$ be a unit vector indicating the velocity of the scene point, S.

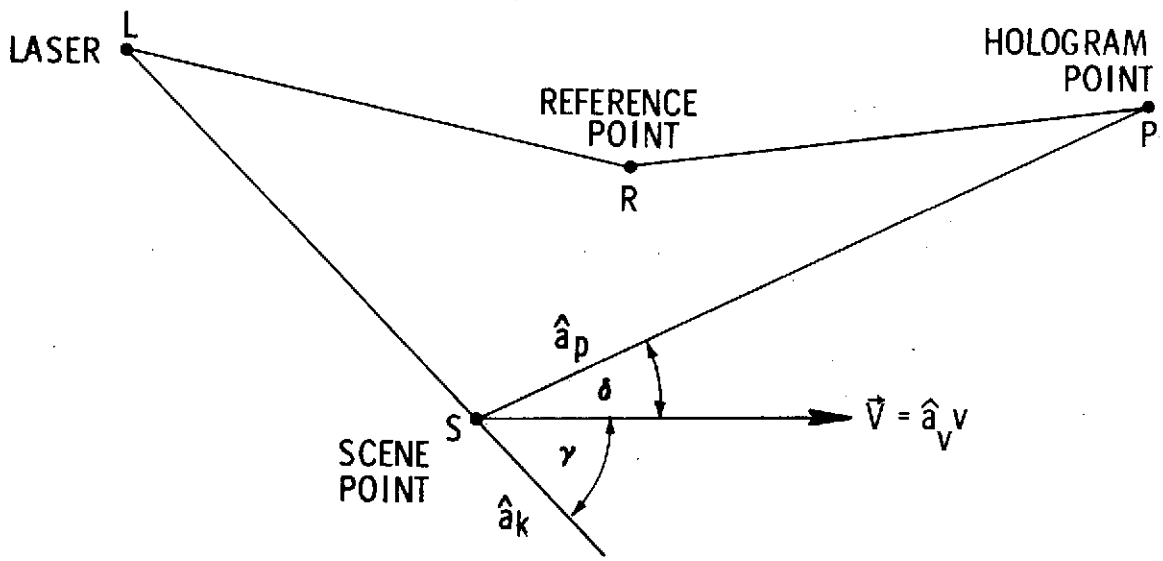

Figure A-2. General geometry for scene-oriented coordinates.

The reference beam is constant in length and composed of two parts, LR + RP. The front illumination beam or scene beam is composed of the two parts, LS + SP. The rate of change of the path length, LS, from the laser to the scene point, S, is given by

$$\vec{V} \cdot \hat{a}_k = v \cos \gamma \quad . \tag{A-10}$$

The rate at which the path length, SP, from the scene point to the hologram point, P, changes is given by

$$\vec{V} \cdot \hat{a}_p = v \cos \delta \quad . \tag{A-11}$$

Therefore, the path length from the laser to the hologram point, P, through scene point, S, is increasing at the rate

$$\frac{ds}{dt} = (\vec{V} \cdot \hat{a}_k - \vec{V} \cdot \hat{a}_p) \quad , \tag{A-12}$$

$$\int_{s_0}^{s} ds = \int_{-\tau/2}^{\tau/2} \vec{V} \cdot (\hat{a}_k - \hat{a}_p)\, dt \quad , \tag{A-13}$$

and

$$s = s_0 + \vec{V} \cdot (\hat{a}_k - \hat{a}_p)\, \tau \quad . \tag{A-14}$$

However, recall that, in general,

$$s = s_0 + f(t) \quad , \tag{A-15}$$

and, in the special case considered previously,

$$s = s_0 + vt \quad ; \tag{A-16}$$

therefore,

$$v = \vec{V} \cdot (\hat{a}_k - \hat{a}_p) \quad .$$

The sinc function for this case may be written as

$$\text{sinc}\left[\frac{k\tau v}{2}\,\hat{a}_v \cdot \left(\hat{a}_k - \hat{a}_p\right)\right] \quad . \tag{A-17}$$

Thus, the exposure at the hologram point, P, for this case becomes

$$\mathcal{E}(P) = m\tau\left\{K_C + E_r E_s \,\text{sinc}\left[\left(\frac{k\tau v}{2}\right)\hat{a}_v \cdot \left(\hat{a}_k - \hat{a}_p\right)\right]\cos\Phi\right\} \quad . \tag{A-18}$$

Looking again at the sinc function of equation (A-17) and performing the indicated scalar products, it is seen that

$$\text{sinc}\left[\frac{k\tau v}{2}\,\hat{a}_v \cdot \left(\hat{a}_k - \hat{a}_p\right)\right] = \text{sinc}\left[\left(\frac{k\tau v}{2}\right)(\cos\gamma - \cos\delta)\right] \quad . \tag{A-19}$$

In this form, the modifying function allows several facts to be noted by inspection. Except for the case of $\tau v = 0$ (i.e., stationary scene, because sinc 0 = 1), the sinc function has a maximum for only the following conditions:

1. That in which $\hat{a}_k$ is parallel to $\hat{a}_p$.

2. That where $\vec{V}$ is perpendicular to the vector $(\hat{a}_k - \hat{a}_p)$.

Consider that the vector $\hat{a}_p$ always points toward the hologram plane (whatever its position); then, the condition that $\hat{a}_k$ and $\hat{a}_p$ be parallel can be met only if $\hat{a}_k$ also points toward the hologram. It is seen that this condition is equivalent to the arrangement for the so-called direct- and diffuse-type holography. This maximum occurs at the point where the incident laser radiation intersects the hologram plane when projected through the scene point. It is noted that the sinc function is a maximum for all orientations of the motion vector, $\vec{V}$.

The second condition for a maximum, that $(\hat{a}_k - \hat{a}_p)$ always be perpendicular to the motion vector, $\vec{V}$, is satisfied for all vectors $(\hat{a}_k - \hat{a}_p)$ lying in a plane perpendicular to $\hat{a}_v$, since, for that condition,

$$\vec{V} \cdot \left(\hat{a}_k - \hat{a}_p\right) = 0 \quad ; \tag{A-20}$$

but,

$$\vec{V} \cdot \left(\hat{a}_k - \hat{a}_p\right) = v(\cos\gamma - \cos\delta) = 0 \quad , \tag{A-21}$$

and this condition is satisfied whenever $\delta = \pm\gamma$. This condition is met by any vector, $\hat{a}_{p0}$, making an angle, γ, with the vector, $\hat{a}_v$. The locus of these vectors, $\hat{a}_p$, forms a circular cone with a half angle equal to γ about the motion vector and contains $\hat{a}_k$ as an element (Fig. A-3).

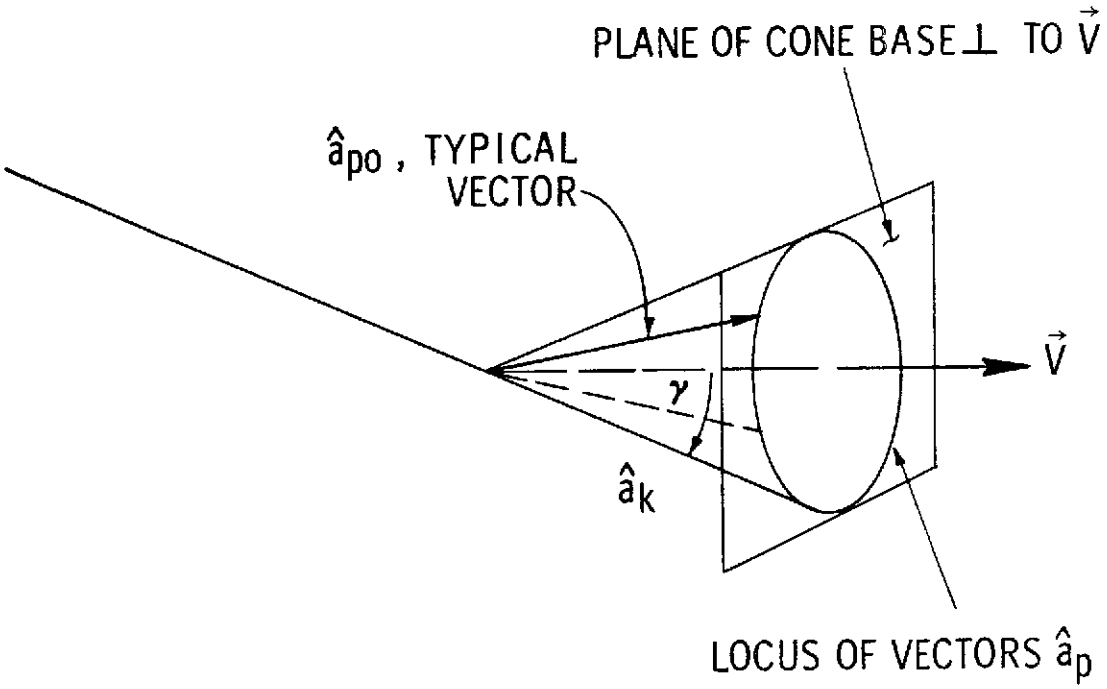

Figure A-3. Cone of constant fringe contrast.

The zeros of the sinc function, equation (A-19), occur for

$$\text{sinc}\left[\frac{\tau k\vec{V}}{2} \cdot \left(\hat{a}_k - \hat{a}_p\right)\right] = \text{sinc } n\,\pi \tag{A-22}$$

$n = \pm 1, 2 \ldots$

Therefore, the zeros occur for

$$\frac{\tau k \vec{V}}{2} \cdot \left(\hat{a}_k - \hat{a}_p\right) = n\pi \quad ; \tag{A-23}$$

i.e.,

$$\vec{V} \cdot \left(\hat{a}_k - \hat{a}_p\right) = \frac{2n\pi}{\tau k} \tag{A-24}$$

or

$$\hat{a}_v \cdot \left(\hat{a}_k - \hat{a}_p\right) = \frac{n\lambda}{v\tau} \quad , \tag{A-25}$$

and

$$\cos\gamma - \cos\delta_{n\pi} = \frac{n\lambda}{v\tau} \tag{A-26}$$

or

$$\cos\delta_{n\pi} = \cos\gamma - \frac{n\lambda}{v\tau} \quad , \tag{A-27}$$

where $\delta_{n\pi}$ is that angle between vectors $\hat{a}_{p0}$ and $\hat{a}_v$ that produces a zero value for the sinc function (i.e., that angle where no fringes will be recorded).

From the above and Figure A-3, it is obvious that if a hologram is formed at any point in space, regions of the hologram having constant fringe contrast will form a conic section, since they represent the intersection of the hologram plane and conical loci mentioned above. If the vector $\hat{a}_p$ is allowed to take on various values, δ, in the range

$$\gamma \leqslant \delta \leqslant \gamma + 2\pi \qquad \text{(A-28)}$$

for a constant $\hat{a}_k$ with angle γ, one can then construct all possible orientations of $\hat{a}_p$ about the motion vector, $\vec{V}$. If for each specific value of δ one allows it to rotate about the velocity vector, $\vec{V}$, then one is able to construct all possible conical loci for $\hat{a}_p$. The results of this are shown in Figure A-4, where three possible values of γ for $\hat{a}_k$ and all possible values of δ for $\hat{a}_p$ for the specific γ are taken. The values of the argument of the sinc function for $\gamma = 0$, $\pi/4$, and $\pi/2$ are then plotted.

Hologram-Oriented Coordinates. In the development of the previous subsection, the exposure was given by

$$\&(P) = m\tau \left\{ K_C + \frac{2E_r E_s}{\tau} \int_{-\tau/2}^{\tau/2} \cos k[s(t) - r]\, dt \right\} \quad . \qquad \text{(A-29)}$$

As before, the form of s(t) must be determined, but now as a function of the hologram. For this development, a fixed-coordinate system is used which has its origin at the center of the hologram and the z-axis normal to the plane of the hologram. This approach or development is the generalized derivation, since it may be used for the region near the hologram as well as the region far from the hologram by simply taking a sufficient number of terms in the series expansions that are developed. Its primary malady is that these very expansions tend to obscure the physical significance of the various steps.

Note the diagram in Figure A-5 and let it be assumed that a hologram is to be formed in the x-y plane of this figure, which is a coordinate system with the origin at the center of the hologram. Analogous to the previous development, let

$$s = s' + S'' \quad ,$$

where s' is the distance from the scene point, P(x,y), of the hologram, and S'' is the distance from the laser source to the scene point, S. (This is simply the total length of illumination called LQ + QP of the previous development.) Then, as before, because of the motion of S, the rate at which S'' changes is

$$\frac{d(S'')}{dt} = \vec{V} \cdot \hat{a}_k = v \cos\gamma \quad .$$

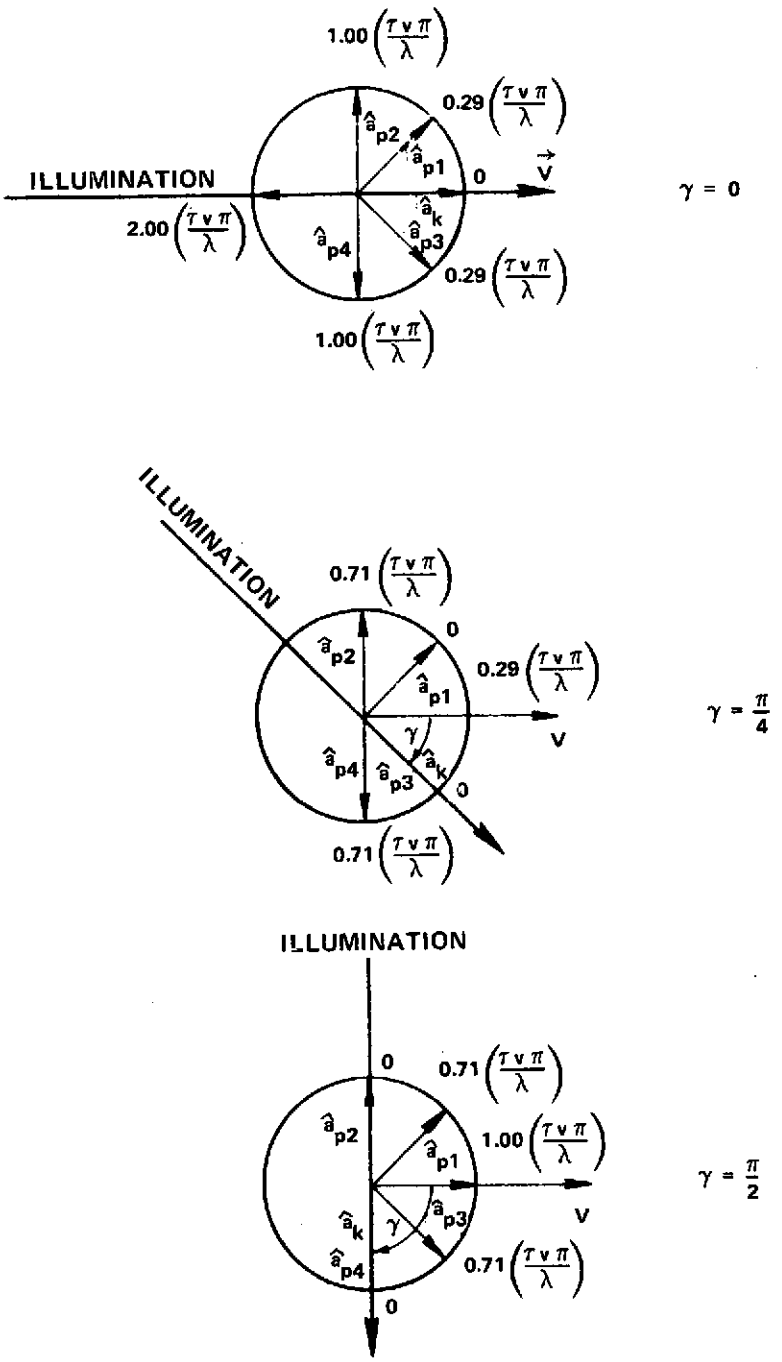

Figure A-4. Variation of sinc function argument with illumination direction.

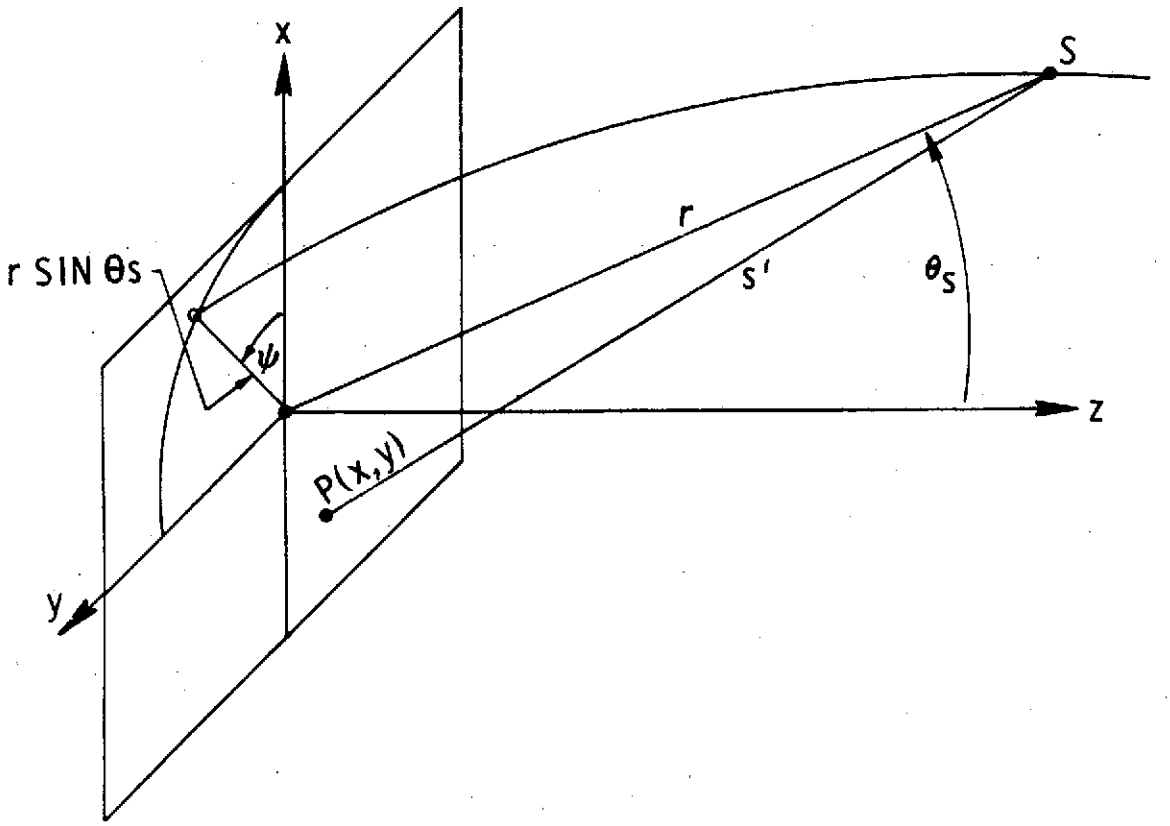

Figure A-5. Hologram-oriented coordinate system.

The coordinates for the point source which may be found from inspection of the diagram (Fig. A-5) are given by

$$x_s = r \sin\theta \cos\Psi \quad ,$$

$$y_s = r \sin\theta \sin\Psi \quad ,$$

and (A-30)

$$z_s = r \cos\theta \quad .$$

Therefore, the distance, s′, from the scene point, S, to a point, P(x,y), of the hologram is

$$s' = \left[(x - x_s)^2 + (y - y_s)^2 + z_s^2\right]^{1/2} , \qquad \text{(A-31)}$$

which becomes

$$s' = r\left(\frac{x^2}{r^2} + \frac{y^2}{r^2} + 1 - \frac{2x}{r}\sin\theta\cos\Psi - \frac{2y}{r}\sin\theta\sin\Psi\right)^{1/2} .$$

By expanding, one obtains

$$\begin{aligned} s' = {} & r\left(1 - \frac{x}{r}\sin\theta\cos\Psi - \frac{y}{r}\sin\theta\sin\Psi\right) + \frac{x^2}{2r^2}\left(1 - \sin^2\theta\cos^2\Psi\right) \\ & + \frac{y^2}{2r^2}\left(1 - \sin^2\theta\sin^2\Psi\right) - \frac{xy}{r^2}\sin^2\theta\sin\Psi\cos\Psi \\ & + \frac{x^3}{2r^2}\left(\sin\theta\cos\Psi - \sin^3\theta\cos^3\Psi\right) \\ & + \frac{x^2y}{2r^2}\left(\sin\theta\sin\Psi - \sin^3\theta\sin\Psi\cos^2\Psi\right) \\ & + \frac{xy^2}{2r^3}\left(\sin\theta\cos\Psi - \sin^3\theta\sin^2\Psi\cos\Psi\right) \\ & + \frac{y^3}{2r^2}\left(\sin\theta\sin\Psi - \sin^3\theta\sin^3\Psi\right) + (\text{higher-order terms}) . \end{aligned} \qquad \text{(A-32)}$$

If one assumes that x/r and y/r are sufficiently small so that only the first-order terms are needed, one obtains

$$s' = r\left(1 - \frac{x}{r}\sin\theta\cos\Psi - \frac{y}{r}\sin\theta\sin\Psi\right) . \qquad \text{(A-33)}$$

To proceed, it becomes necessary to make some assumptions and then investigate some specific examples of the three orthogonal components of motion involved. Following are derivations of the exposures for linear motions of a constant phase laser source, ϕ_s, along each of three orthogonal directions.

For a linear transverse motion (θ), consider the point source, S, to be moving with a constant radius, r_0, and in a constant Ψ plane, called Ψ_0, such that

$$\theta = \theta_0 + \dot{\theta} t \quad ;$$

then,

$$\sin \theta = \sin (\theta_0 + \dot{\theta} t)$$

and

$$\sin \theta = \sin \theta_0 \cos \dot{\theta} t + \cos \theta_0 \sin \dot{\theta} t$$

However,

$$\sin \dot{\theta} t = \dot{\theta} t - \frac{(\dot{\theta} t)^3}{6} + \frac{(\dot{\theta} t)^5}{120} - \ldots \quad ,$$

and

$$\cos \dot{\theta} t = 1 - \frac{(\dot{\theta} t)^2}{2} + \frac{(\dot{\theta} t)^4}{24} - \ldots$$

If it is now assumed that $\dot{\theta} t$ is small enough that only the first term in each series need be used, then one may write

$$\sin \theta = \sin \theta_0 + \dot{\theta} t \cos \theta_0 \quad ;$$

then,

$$\sin^2\theta = \sin^2\theta_0 + 2\dot{\theta}t \sin\theta_0 \cos\theta_0$$

and

$$\sin^3\theta = \sin^3\theta_0 + 3\dot{\theta}t \sin^2\theta_0 \cos\theta_0$$

If these conditions are now substituted into equation (A-32) for the distance, s', one obtains

$$s' = r_0\left[1 - \frac{x}{r_0}(\sin\theta_0 + \dot{\theta}t\cos\theta_0)\cos\Psi_0 - \frac{y}{r_0}(\sin\theta_0 + \dot{\theta}t\cos\theta_0)\sin\Psi_0\right]$$

$$+ \frac{x^2}{2r_0^2}\left[1 - (\sin^2\theta_0 + 2\dot{\theta}t\sin\theta_0\cos\theta_0)\cos^2\Psi_0\right]$$

$$+ \frac{y^2}{2r_0^2}\left[1 - (\sin^2\theta_0 + 2\dot{\theta}t\sin\theta_0\cos\theta_0)\sin^2\Psi_0\right]$$

$$- \frac{xy}{r_0^2}\left[(\sin^2\theta_0 + 2\dot{\theta}t\sin\theta_0\cos\theta_0)\sin\Psi_0\cos\Psi_0\right]$$

$$+ \frac{x^3}{2r_0^3}\left[(\sin\theta_0 + \dot{\theta}t\cos\theta_0)\cos\Psi_0 - (\sin^3\theta_0 + 3\dot{\theta}t\sin^2\theta_0\cos\theta_0)\cos^3\Psi_0\right]$$

$$+ \frac{x^2 y}{2r_0^3}\left[(\sin\theta_0 + \dot{\theta}t\cos\theta_0)\sin\Psi_0 - (\sin^3\theta_0 + 3\,\theta t\sin^2\theta_0\cos\theta_0)\sin\Psi_0\cos^2\Psi_0\right]$$

$$+ \frac{y^3}{2r_0^3}\left[(\sin\theta_0 + \dot{\theta}t\cos\theta_0)\sin\Psi_0 - (\sin^3\theta_0 + 3\,\dot{\theta}t\sin^2\theta_0\cos\theta_0)\sin^3\Psi_0\right]$$

$$+ \text{(higher-order terms)} \quad . \qquad \text{(A-34)}$$

Again, only the first-order terms are taken, and equation (A-34) becomes

$$s' = r_0\left[1 - \frac{x}{r_0}(\sin\theta_0 + \dot{\theta}t\cos\theta_0)\cos\Psi_0 - \frac{y}{r_0}(\sin\theta_0 + \dot{\theta}_s t\cos\theta_0)\sin\Psi_0\right] \quad ,$$

or

$$s' = r_0 - (x\cos\Psi_0 + y\sin\Psi_0)\sin\theta_0 - \dot{\theta}t\,(x\cos\Psi_0 + y\sin\Psi_0)\cos\theta_0 \,.$$

Now, for simplicity, define

$$s_0' \equiv r_0 - (x\cos\Psi_0 + y\sin\Psi_0)\sin\theta_0 \quad ,$$

and one obtains

$$s' = s_0' - \dot{\theta}t\,(x\cos\Psi_0 + y\sin\Psi_0)\cos\theta_0 \quad . \qquad \text{(A-35)}$$

Then, the rate of change of phase between S and P, because of the motion in the θ direction, is

$$\Omega_\theta = k\left(\frac{\partial s'}{\partial t}\right)_\theta = -k V_\theta \left[(x \cos \Psi_0 + y \sin \Psi_0) \frac{\cos \theta_0}{r}\right] \quad , \qquad \text{(A-36)}$$

where

$$V_\theta = \dot{\theta} r \quad .$$

If one proceeds in a similar fashion, the derivations for small motions in the r and Ψ directions may be obtained.

For linear radial motion, r, assume that the point source, S, moves with constant angles, θ_0 and Ψ_0, such that

$$r = r_0 + \dot{r}t \quad ;$$

then,

$$\frac{1}{r} = \frac{1}{r_0 + \dot{r}t}$$

or

$$\frac{1}{r} = \frac{1}{r_0}\left[1 - \frac{rt}{r_0} + \frac{(\dot{r}t)^2}{r_0^2} - \frac{(\dot{r}t)^3}{r_0^3} + \ldots\right] \quad ,$$

and for $\dot{r}t < r_0$,

$$\frac{1}{r^2} = \frac{1}{r_0^2}\left(1 - \frac{2\dot{r}t}{r_0} + \frac{3\,\dot{r}^2 t^2}{r_0^2} - \ldots\right)$$

If the motion, $\dot{r}t$, is small compared with r_0, one may again neglect higher-order terms, and by using the above expressions in equation (A-32), s′ becomes

$$
\begin{aligned}
s' = {} & r_0 + \dot{r}t - x \sin\theta_0 \cos\Psi_0 - y \sin\theta_0 \sin\Psi_0 \\
& + \left[\frac{x^2}{2r_0} (1 - \sin^2\theta_0 \cos^2\Psi_0) + \frac{y^2}{2r_0} (1 - \sin^2\theta_0 \sin^2\Psi_0) \right. \\
& \qquad \left. - \frac{xy}{r_0} \sin^2\theta_0 \sin\Psi_0 \cos\Psi_0 \right] \left(1 - \frac{\dot{r}t}{r_0}\right) \\
& + \left[\frac{x^3}{2r_0^2} (\sin\theta_0 \cos\Psi_0 - \sin^3\theta_0 \cos^3\Psi_0) \right. \\
& \qquad + \frac{x^2 y}{2r_0^2} (\sin\theta_0 \sin\Psi_0 - \sin^3\theta_0 \sin\Psi_0 \cos^2\Psi_0) \\
& \qquad + \frac{xy^2}{2r_0^2} (\sin\theta_0 \cos\Psi_0 - \sin^3\theta_0 \sin^2\Psi_0 \cos\Psi_0) \\
& \qquad \left. + \frac{y^3}{2r_0^2} (\sin\theta_0 \sin\Psi_0 - \sin^3\theta_0 \sin^3\Psi_0 \right] \left(1 - \frac{2\dot{r}t}{r_0}\right)
\end{aligned}
$$

Now, as before, taking only the first-order terms, one obtains

$$
s' = r_0 + \dot{r}t - x \sin\theta_0 \cos\Psi_0 - y \sin\theta_0 \sin\Psi_0 \quad ,
$$

and, considering the direction of k, the phase rate is

$$
\Omega_r = -k \left(\frac{\partial s'}{\partial t} \right)_r \quad ,
$$

$$\Omega_r = -k V_r \qquad \text{(A-37)}$$

where

$$V_r = \dot{r} \quad .$$

For linear transverse motion, Ψ, the third orthogonal component, it is assumed that the point source, S, moves with constant radius, r_0, and angle, θ_0, such that

$$\Psi = \Psi_0 + \dot{\Psi} t \quad ;$$

then,

$$\sin \Psi = \sin \Psi_0 \cos \dot{\Psi} t + \cos \Psi_0 \sin \dot{\Psi} t$$

and

$$\cos \Psi = \cos \Psi_0 \cos \dot{\Psi} t - \sin \Psi_0 \sin \dot{\Psi} t$$

Further,

$$\sin \dot{\Psi} t = \dot{\Psi} t - \frac{(\dot{\Psi} t)^3}{6} + \frac{(\dot{\Psi} t)^5}{120} - \ldots$$

and

$$\cos \dot{\Psi} t = 1 - \frac{(\dot{\Psi} t)^2}{2} + \frac{(\dot{\Psi} t)^4}{24} - \ldots$$

Again, for small motion, $\dot{\Psi} t < \Psi_0$

$$\sin \dot{\Psi} t \approx \dot{\Psi} t$$

and

$$\cos \dot{\Psi} t \approx 1 \quad .$$

Using the proper substitution of these relations in equation (A-32), the following is obtained for s':

$$s' = r_0 \Bigg\{ 1 - \frac{x}{r_0} \sin\theta_0 \cos\Psi_0 - \frac{y}{r_0} \sin\theta_0 \sin\Psi_0 + \frac{x}{r_0} \sin\theta_0 \dot{\Psi} t \sin\Psi_0$$

$$- \frac{y}{r_0} \sin\theta_0 \dot{\Psi} t \cos\Psi_0 + \frac{x^2}{2r_0^2} \left(1 - \sin^2\theta_0 \cos^2\Psi_0\right)$$

$$+ \frac{x^2}{2r_0^2} \sin^2\theta_0 \dot{\Psi} t \sin\Psi_0 \cos\Psi_0 + \frac{y^2}{2r_0^2} \left(1 - \sin^2\theta_0 \sin^2\Psi_0\right)$$

$$- \frac{y^2}{r^2} \sin^2\theta_0 \dot{\Psi} t \sin\Psi_0 \cos\Psi_0 - \frac{xy}{r_0^2} \sin^2\theta_0 \sin\Psi_0 \cos\Psi_0$$

$$- \frac{xy}{r_0^2} \sin^2\theta_0 \dot{\Psi} t \left(\cos^2\Psi_0 - \sin^2\Psi_0\right)$$

$$+ \frac{x^3}{2r_0^3} \Big(\sin\theta_0 \cos\Psi_0 - \dot{\Psi} t \sin\theta_0 \sin\Psi_0 - \sin^3\theta_0 \cos^3\Psi_0$$

$$+ 3 \dot{\Psi} t \sin^3\Psi_0 \cos^2\Psi_0\Big) + \frac{x^2 y}{2r_0^3} \Big[\sin\theta_0 \sin\Psi_0 \dot{\Psi} t \sin\theta_0 \cos\Psi_0$$

$$- \sin^3\theta_0 \sin\Psi_0 \cos^2\Psi_0 + \dot{\Psi} t \sin^3\theta_0 (2 \sin^2\Psi_0 \cos\Psi_0 - \cos^3\Psi_0\Big]$$

$$+ \frac{xy^2}{2r_0^3} \left[\sin\theta_0 \cos\Psi_0 - \dot{\Psi} t \sin\theta_0 \sin\Psi_0 - \sin^3\theta_0 \sin^2\Psi_0 \cos\Psi_0 \right.$$

$$\left. - \dot{\Psi} t \sin^3\theta_0 (2 \sin\Psi_0 \cos^2\Psi_0 - \sin^3\Psi_0) \right]$$

$$+ \frac{y^3}{2r_0^3} (\sin\theta_0 \sin\Psi_0 + \dot{\Psi} t \sin\theta_0 \cos\Psi_0 - \sin^3\theta_0 \sin^3\Psi_0$$

$$\left. - 3 \dot{\Psi} t \sin^3\theta_0 \sin^2\Psi_0 \cos\Psi_0) \right\}$$

Again, taking only first-order terms, one obtains

$$s' = r_0 - x \sin\theta_0 \cos\Psi_0 - y \sin\theta \sin\Psi_0 + \sin\theta_0 \dot{\Psi} t \sin\Psi_0$$

$$- y \sin\theta_0 \dot{\Psi} t \cos\Psi_0 \quad ,$$

and again noting the direction of k,

$$\Omega_\Psi = - k V_\Psi \frac{(x \sin\Psi_0 - y \cos\Psi_0)}{r_0} \quad , \qquad \text{(A-38)}$$

where

$$V_\Psi = \dot{\Psi} r_0 \sin\theta_0 \quad .$$

Any general linear motion may be resolved into the three orthogonal components used in the above development; i.e., (V_r, V_θ, V_Ψ). The constant portion will be a sum of the separate contributions to the phase shifts, and the time-variant portions will be formed by summing the time variant phases found for the three orthogonal components.

The recorded fringe amplitude will then be modified by a sinc function whose argument is

$$\frac{\Omega\tau}{2} = (\Omega_r + \Omega_\theta + \Omega_\Psi)\frac{\tau}{2} \quad .$$

Therefore, combining the time-variant and the constant portions of the phase shifts, the total phase retardation from the laser to the hologram by way of the scene is

$$ks(t) = k\left[S_0'' + \left(\vec{V} \cdot \hat{a}_k\right)\tau\right] + k\,s_0' + (\Omega_r + \Omega_\theta + \Omega_\Psi)\tau \quad ,$$

$$ks(t) = k\left[s_0' + S_0''\right] + (kv\cos\gamma + \Omega)\tau \quad ,$$

$$ks(t) = k\,s_0 + (kv\cos\gamma + \Omega)\tau$$

where

$$\Omega = \Omega_r + \Omega_\theta + \Omega_\Psi \quad . \tag{A-39}$$

The exposure for this case of linear motion may be found by analogy with the exposure for the linear case represented by equation (A-7), where, by analogy, it can be seen that

$$kv \rightarrow kv\cos\gamma + \Omega \quad . \tag{A-40}$$

The exposure for this hologram-oriented coordinate case then becomes

$$\mathcal{E}(P) = m\tau\left\{K_C + E_r E_s \operatorname{sinc}\left[\frac{k\tau}{2}(v\cos\gamma + \Omega)\right]\cos\phi\right\} \tag{A-41}$$

where the constants, m and K_C, are as defined earlier. Then the fringes are modulated by

$$\text{sinc}\left[\frac{k\tau}{2}(v\cos\gamma + \Omega)\right] = \text{sinc}\,\frac{k\tau}{2}\left[v\cos\gamma - \frac{V_\theta}{r}(x\cos\Psi_0 + y\sin\Psi_0)\cos\theta_0 - V_r - \frac{V_\Psi}{r}(x\sin\Psi_0 - y\cos\Psi_0)\right] . \quad \text{(A-42)}$$

This is then the form of the cosine fringe modulation function in terms of the hologram-oriented coordinates.

If one lets $r \to \infty$, the sinc function of equation (A-42) becomes

$$\text{sinc}\left[\frac{k\tau}{2}(v\cos\gamma + \Omega)\right]_\infty = \text{sinc}\left[\frac{k\tau}{2}(v\cos\gamma - V_r)\right] . \quad \text{(A-43)}$$

Recall that δ is the angle between the velocity vector and a unit vector in the radial direction of the previous vector analysis development; then, by analogy,

$$V_r = \vec{V} \cdot \hat{a}_p = v\cos\delta \quad , \quad \text{(A-44)}$$

and equation (A-43) becomes

$$\text{sinc}\left[\frac{k\tau}{2}(v\cos\gamma + \Omega)\right]_\infty = \text{sinc}\left[\frac{k\tau v}{2}(\cos\gamma - \cos\delta)\right] , \quad \text{(A-45)}$$

and one has the expected result.

Resultant Effects of Linear Motion on the Reconstructed Wavefront

The previous section complements this section in showing that the effect of motion of a point source scene during the formation of a hologram is a modification of the recorded fringe contrast at various points of the hologram. Furthermore, the effects on the hologram's recorded fringes caused by the scene motion may be derived by considering the motion of only a single point of a rigid moving scene.

Now the characteristics of the image reconstructed from a hologram having such motion-modified fringes will be investigated. A comparison of this image with the original object will give a point-spread function for the motion holography case. The approach followed will be that of the currently existing method presented in Reference 12.

Consider Figure A-6, where a particular source distribution in the vicinity of the scene is assumed. It is desirable then to find the resulting amplitude and phase distribution on the hologram at point Q. If it can be shown that this is identical to the amplitude and phase distribution of the reconstructed field, it will prove that the assumed source will describe the reconstructed virtual image. One chooses a uniform line source lying along the motion vector as the assumed source (Fig. A-6), i.e., the Z-axis in this diagram. The uniform line source of the length, $\Delta\ell$, is centered at the t = 0 scene point, s_0, and has a linear phase variation, kbz, where b is some proportionality constant. The resulting field will be symmetrical with respect to revolution about the Z-axis. Then, it is desired to know the field at a point, Q, on the hologram, a distance, $q_0 >> \Delta\ell$, from the source and at an angle, δ, from the Z-axis.

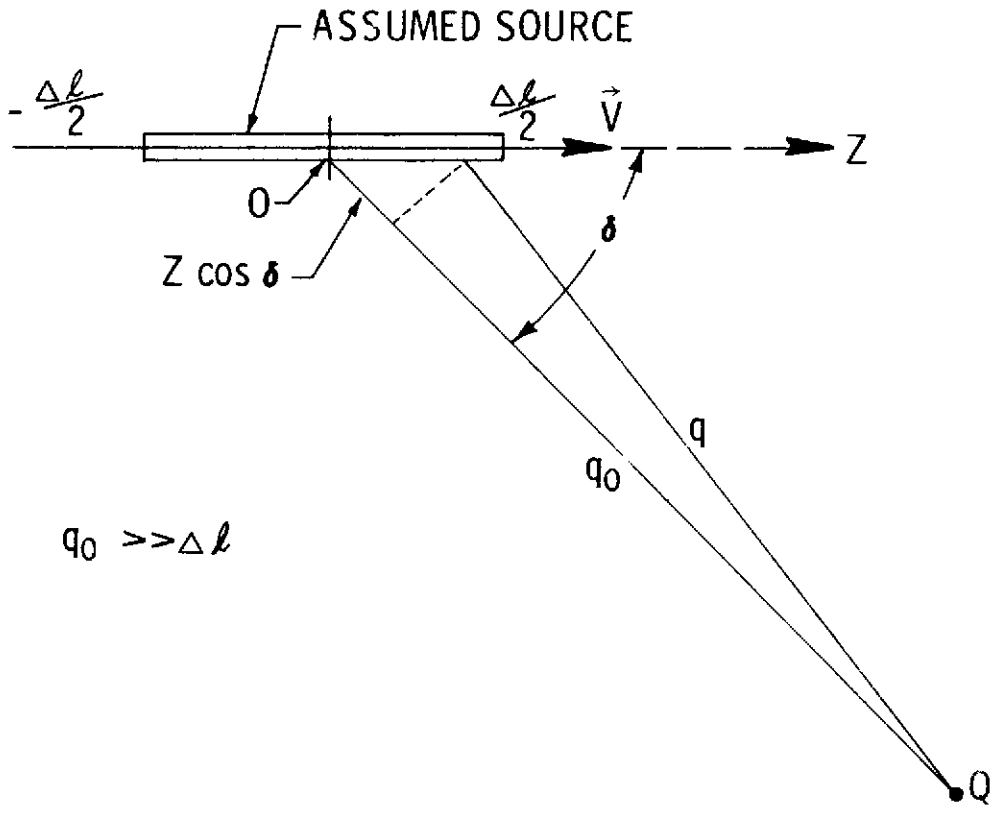

Figure A-6. Geometry for reconstruction analysis.

We consider that the field $d\vec{E}$ at the point, Q, is due to the contributions of point sources in the infinitesimal length, dZ, at a distance, Z, from the origin. Then, $d\vec{E}$ is given by

$$d\vec{E} = \frac{A}{q_0} \exp [i(\omega t + kbZ - kq)] \, dZ \quad . \tag{A-46}$$

From the diagram,

$$q_0 = q + Z \cos \delta \quad ; \tag{A-47}$$

thus,

$$q = q_0 - Z \cos \delta \quad .$$

Then,

$$d\vec{E} = \frac{A}{q_0} \exp [i(\omega t + kbZ - kq_0 + kZ \cos \delta)] \, dZ \quad , \tag{A-48}$$

where A is a constant involving amplitude.

Now, by integrating, one finds the total field at Q

$$\vec{E}(Q) = \frac{A}{q_0} \exp i (\omega t - kq_0) \int_{\Delta \ell/2}^{\Delta \ell/2} \exp [ik (b - \cos \delta) Z] \, dZ \quad . \tag{A-49}$$

Applying Euler's formula to the integral and setting in the limits of integration,

$$\vec{E}(Q) = \frac{A}{q_0} \exp i(\omega t - kq_0) \left\{ \frac{2 \sin [k (b - \cos \delta) \frac{\Delta \ell}{2}}{k (b - \cos \delta)} \right\} \quad . \tag{A-50}$$

Upon multiplying the brackets by $\Delta\ell/\Delta\ell = 1$,

$$\vec{E}(Q) = \frac{A}{q_0} \exp i(\omega t - kq_0)\, \Delta\ell\, \text{sinc}\left[k(b - \cos\delta)\frac{\Delta\ell}{2}\right] \quad . \tag{A-51}$$

Therefore, E(Q) represents a homocentric wave, centered at the origin point, 0, with an amplitude weighting given by

$$\text{sinc}\left[\frac{k\Delta\ell}{2}(b - \cos\delta)\right] \quad . \tag{A-52}$$

Equation (A-51) is the description of the field at the point, Q, of the hologram plane resulting from the assumed source of a uniform line.

It is now appropriate to determine the amplitude and phase distribution of the hologram's reconstructed field and then compare the reconstructed (virtual image) field with that of the assumed source. If the two are identical, it will be obvious that the assumed source will describe the reconstructed virtual image.

For the reconstructed hologram, the amplitude transmission factor may be written as

$$T_a = T_0 - k_f \mathcal{E} \quad . \tag{A-53}$$

The exposure, $\mathcal{E}$, is given by equation (A-18),

$$\mathcal{E} = m\tau\left\{K_C + E_r E_s \,\text{sinc}\left[\frac{k\tau\vec{V}}{2} \cdot \left(\hat{a}_k - \hat{a}_p\right)\right] \cos(\phi_r - \phi_s)\right\} \quad ,$$

or

$$\mathcal{E} = K_1 + K_2 \,\text{sinc}\left[\frac{k\tau\vec{V}}{2} \cdot \left(\hat{a}_k - \hat{a}_p\right)\right] \cos(\phi_r - \phi_s) \quad . \tag{A-54}$$

Then, from the amplitude transmission factor, one can write

$$T_a = T_0 - k_f \left\{ K_1 + K_2 \operatorname{sinc} \left[\frac{k\tau \vec{V}}{2} \cdot \left(\hat{a}_k - \hat{a}_p \right) \cos \left(\phi_r - \phi_s \right) \right] \right\}$$

or

$$T_a = T_0 - K_1' + K_2' \operatorname{sinc} \left[\frac{k\tau \vec{V}}{2} \cdot \left(\hat{a}_k - \hat{a}_p \right) \cos \left(\phi_r - \phi_s \right) \right] \quad . \quad \text{(A-55)}$$

Now, since equations (A-53), (A-54), and (A-55) describe the exposure and development of the field resulting from a motion scene, the reconstructed virtual image field (first-order diffraction) has an amplitude proportional to the magnitude of the spatial variations in the amplitude transmission factor and is, therefore, proportional to

$$\operatorname{sinc} \left[\frac{k\tau \vec{V}}{2} \cdot \left(\hat{a}_k - \hat{a}_p \right) \right] = \operatorname{sinc} \left[\frac{kv\tau}{2} \left(\cos \gamma - \cos \delta \right) \right] \quad . \quad \text{(A-56)}$$

Therefore, since the fringe phase $(\Phi_r - \Phi_s)$ is independent of the motion, $\vec{V}$, the hologram will reconstruct a homocentric wave with the center at the t=0 position of the scene point.

Then, comparing equations (A-52) and (A-56), one sees that, if $\Delta \ell = v\tau$ and $b = \cos \gamma$, the phase fronts and amplitude distributions are identical for the assumed source and the reconstructed (virtual image) field of the hologram. Therefore, the virtual image will be a line source of length, $v\tau$, and with a phase equal to $KZ \cos \gamma$, where Z is the distance from the center of the source. In other words, the image will have the same blur as results from any detector (such as a conventional photograph) having an integrating time of τ. Furthermore, the phase relationships are preserved between the impulses that sequentially formed the hologram.

REFERENCES

1. Hollinden, A.B.; and Eaton, L.R.: Feasibility Study of a Zero-Gravity (Orbital) Atmospheric Cloud Physics Experimental Laboratory. NASA CR-128998, November 1972.

2. Eaton, L.R.; Greco, R.V.; and Hollinden, A.B.: Zero-Gravity Cloud Physics Laboratory Candidate Experiments Definition and Preliminary Concept Studies. NASA-CR 129002, June 1973.

3. Eaton, L.R.; and Greco, R.V.: Zero-Gravity Cloud Physics Laboratory Experiment Program Definition and Preliminary Laboratory Concept Studies. NASA-CR 129013, September 1973.

4. Kurtz, Robert L.: The Techniques of Holographic Particle Sizing. NASA TR R-404, March 1973.

5. Kurtz, Robert L., et al.: A Holographic Technique for Recording a Hypervelocity Projectile with Front Surface Resolution. Applied Optics, Vol. 9, No. 5, May 1970.

6. Kurtz, Robert L., et al.: Experimental Investigation of a Holographic System that Records Front Surface Detail from a Scene Moving at High Velocities. Applied Optics, Vol. 11, No. 9, September 1972.

7. Kurtz, Robert L., et al.: A Holographic System that Records Front Surface Detail of a Scene at High Velocity. NASA TR R-380, January 1972.

8. Kurtz, Robert L., et al.: Holographic Motion Picture Camera that Allows Front Surface Detail to be Recorded in Real Time Using a Continuous Wave Laser. Applied Optics, Vol. 12, No. 4, April 1973.

9. Kurtz, Robert L.: Hybrid Holographic System. U.S. Patent No. 3,535,014, June 1972.

10. Kurtz, Robert L.: Multiple patents on holography. MFS Case Nos. 21704, 20074, 20596, 21087, 22517, 22537, and 22434. Office of Patent Counsel (A&PS-PAT) Marshall Space Flight Center, Huntsville, Ala.

11. Collier, R.J.; Burkhardt, C.B.; and Lin, L.H.: Optical Holography. The Academic Press, New York, 1971.

12. Neumann, Don B.: Holography of Moving Scenes. Journal of the Optical Society of America, Vol. 58, No. 4, April 1968.